Quaternary

Neogene

Paleogene

Cretaceous

Jurassic

Triassic

Permian

Carboniferous

Devonian

Silurian

Ordovician

Cambrian

Proterozoic

Volume 4

Chapter 4

THE GEOLOGY OF **COLOMBIA**

SERVICIO GEOLÓGICO COLOMBIANO

Paipa Geothermal System, Boyacá: Review of Exploration Studies and Conceptual Model

Claudia María ALFARO–VALERO[1]* (ID), Jesús Bernardo RUEDA–GUTIÉRREZ[2] (ID), Jhon Camilo MATIZ–LEÓN[3] (ID), Miguel Angel BELTRÁN–LUQUE[4] (ID), Gilbert Fabián RODRÍGUEZ–RODRÍGUEZ[5] (ID), Gina Z. RODRÍGUEZ–OSPINA[6] (ID), Carlos Eduardo GONZÁLEZ–IDÁRRAGA[7] (ID), and Jaison Elías MALO–LÁZARO[8] (ID)

Abstract The Paipa geothermal system is located at 2525 masl in a terrain tilted from south to north towards the Chicamocha River, where the geology is dominated by sedimentary rocks intruded by felsic magmas. The Miocene and Pleistocene volcanic activity produced pyroclastic deposits and dome complexes. A deep saline sodium sulfate water, presumably originating from the infiltration of meteoric water followed by dissolution of an evaporite, mixes with geothermal fluid. This process masks the chemical and isotopic composition of the geothermal component of fluid discharge in hot springs, the temperatures of which reach 76 °C. Organic and magmatic/mantle contributions also affect the composition of the gas phase discharges. High concentrations of radioactive elements are found in the area, mainly in El Durazno Intrusive, a highly altered intrusion located to the west. Extensive outcrops of the Une Formation at high elevation (2900 masl) in the Tibasosa–Toledo Anticline represent the main recharge zone. High angle faults (Las Peñas, Paipa–Iza, and Agua Tibia Faults) and the contacts between the magmatic intrusions and the surrounding metamorphic and sedimentary rocks control the permeability of the fractured reservoir. Northward, rising hot water encounters elevated permeability in sedimentary rocks, mainly in the Une Formation, forming a sedimentary reservoir. The subsequent fluid outflow is facilitated by a normal subvertical NW fault (Cerro Plateado Fault). Two main discharge zones, Instituto de Turismo de Paipa–Lanceros and La Playa, are controlled by intersections between faults and permeable rocks.

Keywords: *geothermal exploration, hot springs, geothermal conceptual model, Paipa geothermal system.*

Resumen El sistema geotérmico de Paipa se encuentra a 2525 m s. n. m. en un terreno inclinado de sur a norte hacia el río Chicamocha, donde la geología está dominada por rocas sedimentarias intruidas por rocas magmáticas félsicas. La actividad volcánica del Mioceno y Pleistoceno produjo depósitos piroclásticos y complejos de domos. Un circuito profundo de agua salina sulfatada sódica, presumiblemente originado por la infiltración de agua meteórica seguida por la disolución de una evaporita, se mezcla con fluido geotérmico. Este proceso de mezcla enmascara la composición química e isotópica de la descarga acuosa de los manantiales termales,

1 calfaro@sgc.gov.co
  Servicio Geológico Colombiano
  Dirección de Geociencias Básicas
  Diagonal 53 n.° 34–53
  Bogotá, Colombia

2 jbrueda@sgc.gov.co
  Servicio Geológico Colombiano
  Dirección de Geociencias Básicas
  Diagonal 53 n.° 34–53
  Bogotá, Colombia

3 jmatiz@sgc.gov.co
  Servicio Geológico Colombiano
  Dirección de Geociencias Básicas
  Diagonal 53 n.° 34–53
  Bogotá, Colombia

4 mbeltran@sgc.gov.co
  Servicio Geológico Colombiano
  Dirección de Geociencias Básicas
  Diagonal 53 n.° 34–53
  Bogotá, Colombia

5 gfrodriguez@sgc.gov.co
  Servicio Geológico Colombiano
  Dirección de Geociencias Básicas
  Diagonal 53 n.° 34–53
  Bogotá, Colombia

6 grodriguezo@sgc.gov.co
  Servicio Geológico Colombiano
  Dirección de Geociencias Básicas
  Diagonal 53 n.° 34–53
  Bogotá, Colombia

7 cegonzalezi@sgc.gov.co
  Servicio Geológico Colombiano
  Dirección de Geociencias Básicas
  Diagonal 53 n.° 34–53
  Bogotá, Colombia

8 jmalo@sgc.gov.co
  Servicio Geológico Colombiano
  Dirección de Geociencias Básicas
  Diagonal 53 n.° 34–53
  Bogotá, Colombia

* Corresponding author

cuya temperatura alcanza los 76 °C. Aportes de fuente orgánica y magmática/mantélica también afectan la composición de las descargas en fase gaseosa. Concentraciones altas de elementos radiactivos se encuentran en el área, principalmente en El Durazno, una intrusión con alteración intensa ubicada al oeste. Extensos afloramientos de la Formación Une localizados a mayor elevación (2900 m s. n. m.) en el Anticlinal de Tibasosa–Toledo conforman la principal zona de recarga. Fallas de alto ángulo (fallas de Las Peñas, Paipa–Iza y Agua Tibia) y los planos de contacto entre intrusiones magmáticas y las rocas metamórficas y sedimentarias que las rodean controlan la permeabilidad del reservorio fracturado. Más al norte, el flujo ascendente causado por flotabilidad del agua caliente encuentra alta permeabilidad en rocas sedimentarias, principalmente de la Formación Une, formando un reservorio sedimentario. La circulación lateral posterior del fluido es favorecida por una falla normal subvertical NW (Falla de Cerro Plateado). Dos zonas de descarga principales, Instituto de Turismo de Paipa–Lanceros y La Playa, son controladas por la intersección entre fallas y rocas permeables.

Palabras clave: *exploración geotérmica, fuentes termales, modelo conceptual geotérmico, sistema geotérmico de Paipa.*

1. Introduction

The Colombian convective geothermal systems are located in the Andean Region. At least 12 geothermal areas have been identified (Figure 1a), which include (1) the Cerro Bravo–Cerro Machín Volcanic Complex, which comprises the zones of Nereidas–Botero Londoño and the Villa María Fault in the Nevado del Ruiz Volcano, Laguna del Otún in the Santa Isabel Volcano, Santa Rosa–San Vicente in the vicinity of the Paramillo de Santa Rosa Volcano, and the Cerro Bravo Volcano and Cerro Machín Volcano (Geocónsul, 1992); (2) the Chiles–Cerro Negro Volcanic Complex; (3) the Azufral Volcano; (4) the Paipa–Iza geothermal area; (5) the Cumbal Volcano; (6) the Galeras Volcano; (7) the Puracé Volcano; (8) the Sotará Volcano; (9) the Doña Juana Volcano; (10) and the Nevado del Huila Volcano. The geothermal areas numbered 2 to 10 were identified through a national assessment study of geothermal resources in Colombia (Organización Latinoamericana de Energía, Instituto Colombiano de Energía Eléctrica, Consultoría Tecnológica Colombiana & Geotérmica Italiana, 1982). In addition, there are the (11) San Diego geothermal area and (12) Sibundoy Volcano, the geothermal systems of which were identified from the hot springs national inventory project (Servicio Geológico Colombiano, 2015). Currently, five of those systems are being investigated for geothermal exploration: Nevado del Ruiz by CHEC–EPM, ISAGEN, and the Servicio Geológico Colombiano (SGC) (Alfaro, 2015); Chiles–Cerro Negro by ISAGEN–CELEC (Alfaro, 2015); and the Azufral Volcano, San Diego, and Paipa areas by the SGC (Alfaro et al., 2015, 2017; Rueda & Rodríguez, 2016). Other conductive geothermal systems could be hosted in sedimentary basins having high conductive heat flows, particularly in the Eastern Llanos, Eastern Cordillera, Caguán–Putumayo, Catatumbo, and Cesar Ranchería Basins (Figure 1b; Alvarado et al., 2008).

The Paipa geothermal system has had an intermediate–high exploration priority since the national assessment studies of geothermal resources in Colombia (Organización Latinoamericana de Energía, Instituto Colombiano de Energía Eléctrica, Consultoría Tecnológica Colombiana & Geotérmica Italiana, 1982).

The Grupo de Investigación y Exploración de Recursos Geotérmicos of the SGC has carried out several exploration studies in geology, geochemistry, geophysics, and modeling. These results are integrated into a conceptual model presented in this chapter.

2. Background

The Paipa geothermal system is located on the high plateau of the Eastern Andean Cordillera, south of the town of the same name and from the Chicamocha River to the west of the Tibasosa–Toledo Anticline (Figure 2).

The first studies of this system included fluid geochemistry and geology (Bertrami et al., 1992; Boussingault & Rolin, 1849; Empresa Nacional de Uranio S.A. & Instituto de Asuntos Nucleares, 1979, 1980; Ferreira & Hernández, 1988; Garzón, 2003; Hernández & Osorio, 1990; Navia & Barriga, 1929; Organización Latinoamericana de Energía, Instituto Colombiano de Energía Eléctrica, Consultoría Tecnológica Colombiana & Geotérmica Italiana, 1982;Renzoni & Rosas, 1967; Renzoni et al., 1998).

At least three conceptual models of the Paipa geothermal system have been proposed in the past. Based on geological observations and fluid geochemistry, Ferreira & Hernández (1988) formulated a model with a magmatic heat source hosted in the sedimentary sequence, inferred from the Olitas, Pan de Azúcar, and El Durazno volcanic bodies. A reservoir of primary perme-

Quaternary
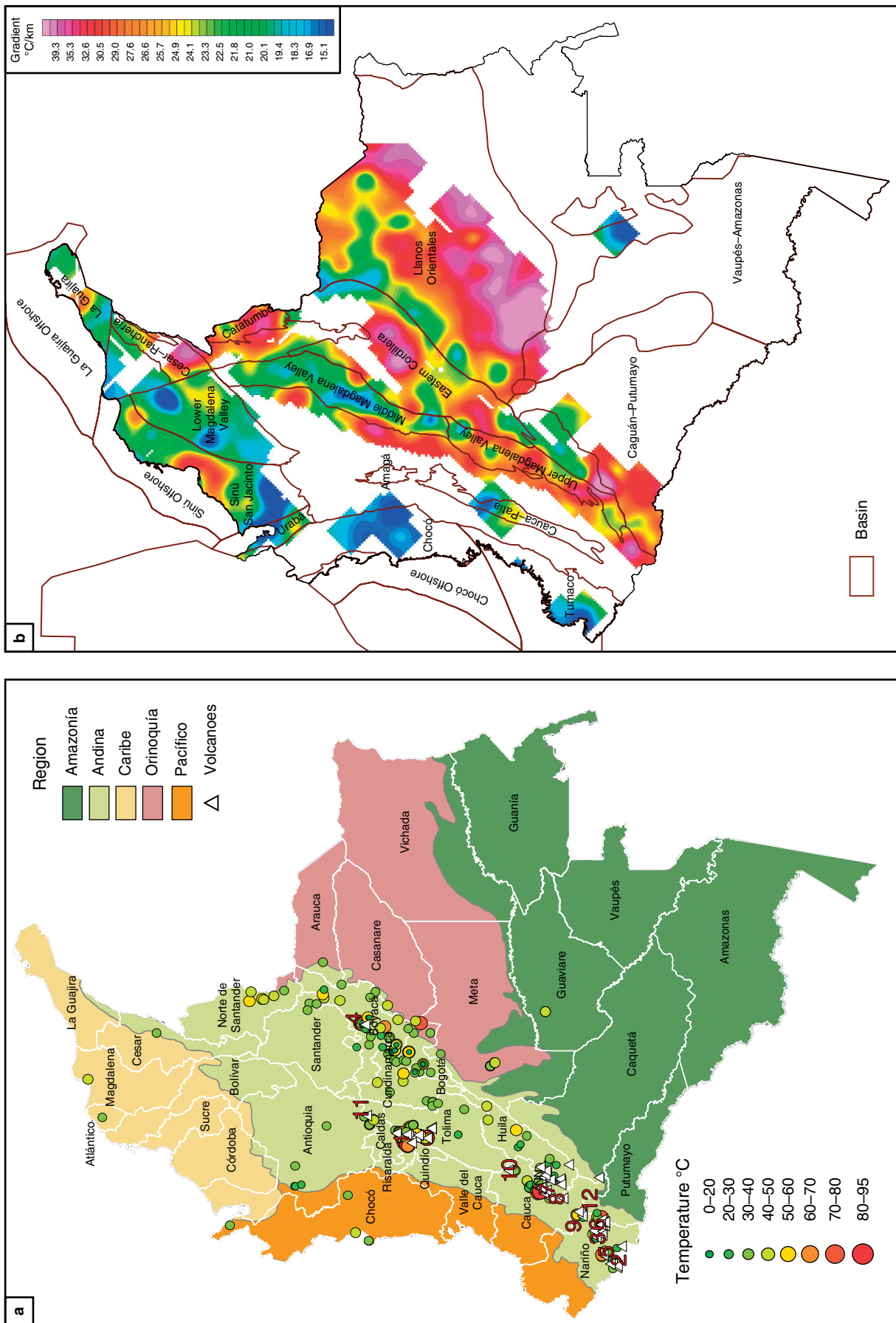
Figure 1. Geothermal resources from Colombia. **(a)** Convective hydrothermal systems (Geocónsul, 1992; Organización Latinoamericana de Energía, Instituto Colombiano de Energía Eléctrica, Consultoría Tecnológica Colombiana & Geotérmica Italiana, 1982; Servicio Geológico Colombiano, 2015). Geothermal areas: (1) the Cerro Bravo–Cerro Machín Volcanic Complex, (2) the Chiles–Cerro Negro Volcanic Complex, (3) the Azufral Volcano, (4) the Paipa–Iza geothermal area, (5) the Cumbal Volcano, (6) the Galeras Volcano, (7) the Puracé Volcano, (8) the Sotará Volcano, (9) the Doña Juana Volcano, (10) the Huila Volcano, (11) San Diego geothermal area, (12) Sibundoy Volcano. **(b)** Geothermal gradient map (Alvarado et al., 2008).
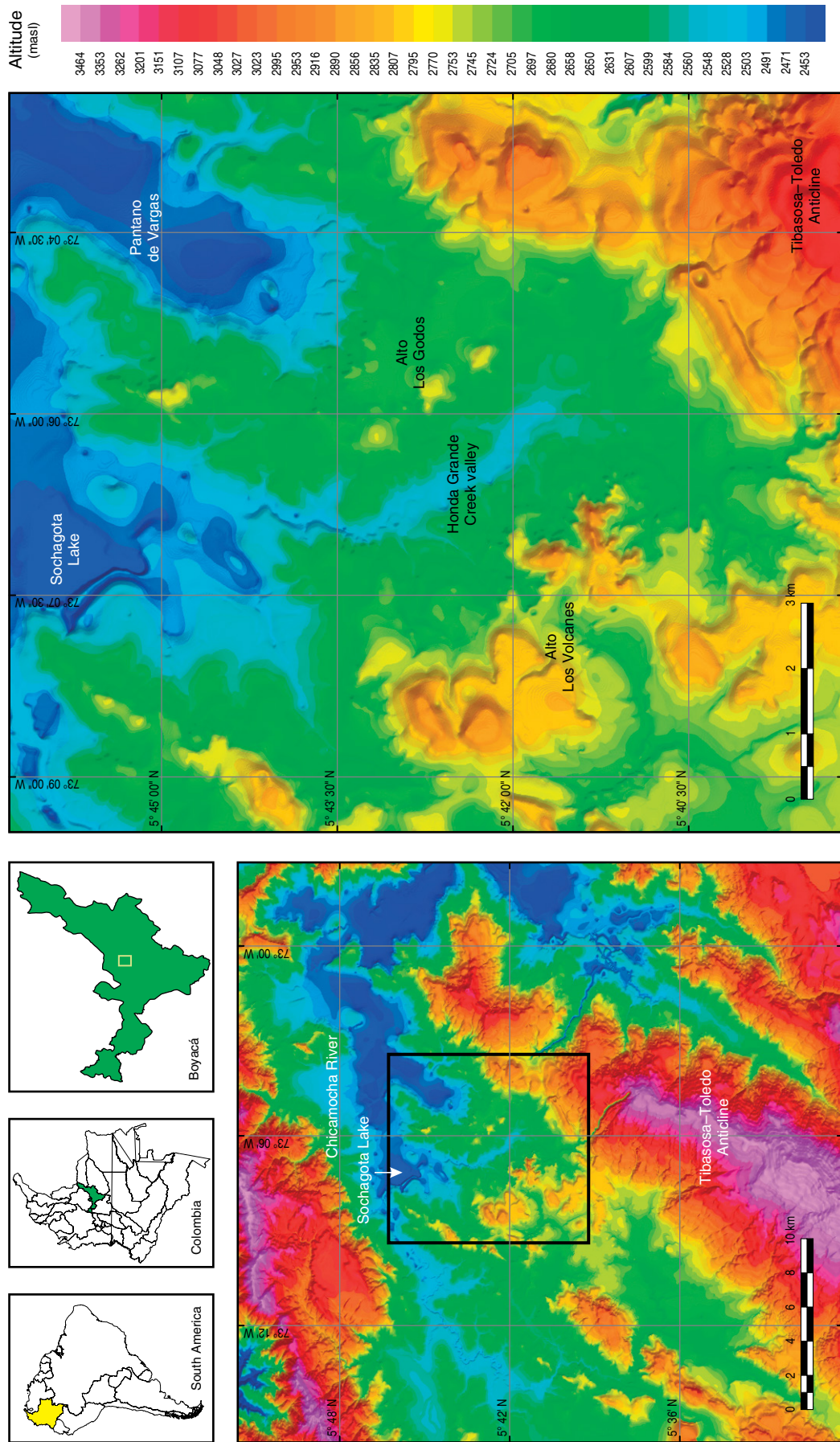
Figure 2. Location of the Paipa geothermal area.

ability occurs in the white sandstones of the Une Formation, and shallow aquifers occur in the Labor y Tierna Formations. A clay layer from the Churuvita Group forms the cap rock, and a recharge zone infiltrates through the Une Formation. The discharge zone is fed by deep fluids transmitted through NE–SW deep normal faults, and the reservoir temperature is above 200 °C based on cation aqueous geothermometers.

According to Lozano (1990), from the integration of geological information and a resistivity survey performed by the Instituto Colombiano de Energía Eléctrica (ICEL) and the Electrificadora de Boyacá, a magmatic heat source is located between 3 and 5 km depth, which is related to volcanism; the system also has two reservoirs. The first is shallow and located within the Guadalupe Group and its impermeable layer would be the Guaduas Formation. The second reservoir is deeper (at 1000 to 1200 m) and thicker, and it is hosted in the Churuvita Group and the Une Formation; its impermeable layer would be the Conejo Formation. According to this work, the most interesting area in the resource's location has been identified from the resistivity survey, which is located in the depression of Sochagota Lake, where it is elongated in a NE direction and has a resistivity between 10 and 20 Ω·m.

In the last 15 years, the SGC accomplished the following studies: (1) geological mapping at a scale of 1:25 000 and a structural model (Velandia, 2003), including a map of volcanic units (Cepeda & Pardo, 2004); (2) chemical and isotopic characterization of hot spring waters (Alfaro, 2002a, 2002b); (3) a preliminary resistivity survey (Vásquez, 2002); (4) a radon survey (Alfaro & Espinosa, 2004); and (5) preliminary hydrothermal alteration and gas studies (Alfaro, 2005a, 2005b). From the integration of those studies, a conceptual model was proposed (Alfaro et al., 2005), in which the system is hosted in a volcanic caldera and the heat source comprises cooling plutons that are 2.1–2.5 Ma. A deep reservoir likely occurs in fractured rocks associated with basement faults (Paipa–Iza and Cerro Plateado Faults), which were also conduits for magmas. Shallower reservoirs are potentially hosted in the sedimentary sequence, which because of their lateral extension allow the geothermal water to flow northwards up to the surface discharge zone. The geothermal fluid has been heated to more than 300 °C by deep circulation. The fluid discharge zone is structurally controlled by fault intersections related to the rotation of blocks defined by Velandia (2003). The outflow goes from south to north up to the main discharge zone in the ITP–Lanceros sector. The hot spring water is not representative of the reservoir fluid because its chemical and isotopic composition is masked by mixing with a low temperature saline sodium sulfate source and by a contribution of an organic gas.

Complementary studies were performed by the SGC, most of which were related to the geothermal exploration, including uranium exploration (González et al., 2008), a cold and hot springs inventory (Ortiz & Alfaro, 2010), surface hydrother-

mal alteration, isotopic investigation of groundwater (Alfaro, 2012), potential field surveys (Vásquez, 2012), a geoelectrical survey (Franco, 2012), and a magnetotelluric study (González–Idárraga & Rodríguez–Rodríguez, 2017, Anexo A). From these new studies, an updated conceptual model was formulated (Alfaro, 2015). The regional recharge likely comes from the western flank of the Tibasosa–Toledo Anticline through the Une Formation. El Durazno Intrusive is a magmatic intrusion, and it could contribute some of the heat from radiogenic heat due to the relatively high concentrations of ^{238}U, ^{232}Th, and ^{40}K. The most significant hydrothermal alteration on surface is of the argillic and advanced argillic type in El Durazno Intrusive. Geophysical contrasts in the complete Bouguer anomaly define the Paipa–Toca Fault, which has a N–S direction, and a lineament called the Firavitoba Fault, as previously identified by Velandia (2003). The low resistivity anomalies from the shallow surveys are attributed to saline pore waters in the Churuvita Formation, south of the intersection between the Buenavista and Rancho Grande Faults. Lastly, three resistivity structures were identified: a very high resistivity zone that corresponds to the center of the Tibasosa–Toledo Anticline, a shallower low resistivity zone possibly related to a clay–rich layer or an aquifer filled with saline water, and an intermediate resistivity zone characteristic of the sedimentary rocks that could host a geothermal reservoir.

3. Materials and Methods

This work is directed at developing a conceptual model based on the integration of a 3D geological model that is constrained by gravity and magnetic surveys, with magnetotelluric models. These were used to determine the lithologic and structural controls on the localization of reservoirs of hot water and their relation to igneous intrusions, which might be heat sources and influence fluid flow through the hydrothermal system. Fluid geochemistry, vertical electrical sounding, rock radioactive elements analysis, soil temperature measurements, and geochronologic data were integrated as part of the model. The integration of the results was performed through workshops with participation from the scientific team comprising coauthors of this chapter. The methods for the specific surveys can be found in the references cited.

4. Results

4.1. Geology

The regional geology is represented in maps at a scale of 1:100 000, which show the predominance of Jurassic, Cretaceous, and Paleogene sedimentary units, with evidence of volcanism represented by andesite rocks (Renzoni & Rosas, 1967; Renzoni et al., 1998).

The basement comprises metamorphic rocks (phyllites, schists, and gneisses) intruded, at least in the sector where the basement is exposed, by Paleozoic and Mesozoic plutons including Chuscales, Otengá, Santa Rosita, and Aguachica. These units are presumably overlain in the study area by the Devonian – Carboniferous sedimentary sequences of the Tibet, Floresta, and Cuche Formations (Mojica & Villaroel, 1984).

The Paipa area is locally covered by sedimentary sequences of Cretaceous and Paleogene ages over a basement that does not crop out in the studied area (Figure 3; Velandia, 2003). The Tibasosa unit in the SE area comprises gray shales, limestones, and sandstones. The Une Formation consists principally of sandstones that are fine to coarse grained with conglomerate lenses and intercalations of gray shales. The Churuvita Group comprises shales and quartz sandstone. The Conejo Formation comprises thick layers of black shales with layers of fine–grained quartz sandstones. Thin layers of siliceous siltstones and mudstones with phosphorite–rich layers that show intense fracturing in outcrops compose the Plaeners Formation. Los Pinos Formation comprises black and green siltstones and thin to medium interlayers of sandstones. The Labor y Tierna Formation comprises fine and coarse–grained sandstones. The Guaduas Formation is made of interbedded claystones, quartz sandstones, and coal layers. Quartz sandstones with layers of claystone compose the Bogotá Formation. The Tilatá Formation is the youngest unit and comprises unconsolidated sandy sedimentary deposits. Overlying the Tilatá Formation, there are Quaternary alluvial deposits.

Several investigations of the Paipa Volcano (Ferreira & Hernández, 1988; Garzón, 2003; Hernández & Osorio, 1990; Navia & Barriga, 1929; Renzoni & Rosas, 1967) describe the geology and geochemistry of this atypical volcanic center in the Eastern Cordillera.

Cepeda & Pardo (2004) proposed the existence of a volcanic caldera and associated deposits comprising air fall, a debris flow, pyroclastic flows, and rhyolitic flow domes (Figure 3). The first episode involved the construction of a volcanic edifice, which was followed by caldera collapse (Cepeda & Pardo, 2004). The products include block and ash flows, lavas, and pyroclastic deposits.

Rueda (2017), based on Ferreira & Hernández (1988), Garzón (2003), Hernández & Osorio (1990), and new field observations, added the domes unit to the geological map of the Paipa area (Figure 3, red polygons) and divided it into three areas, which are the alto Los Volcanes, Honda Grande Creek, and alto Los Godos (Figures 3, 4a, 4b). The rocks from the alto Los Godos and some from the alto Los Volcanes are interpreted as ignimbrites and were produced in the first volcanic episode of the area (Cepeda & Pardo, 2004). However, the geomorphological, petrographic, geochemical, and geochronological data indicate that these units comprise rhyolites and trachydacites, with a calc–alkaline signature (Peccerillo & Taylor, 1976), and

they are classified as volcanic arc granites (VAG) in the Pearce et al. (1984) diagram (Figure 4c–e). Anorthoclase, sanidine, albite, and subordinate biotite and hornblende make up the phenocrysts. The matrix is mostly cryptocrystalline, with varying amounts of glass replacing the feldspar cores. Cepeda & Pardo (2004) reported ages of 2.13 ± 0.39 to 2.29 ± 0.17 Ma for one of the domes of the alto Los Volcanes. Ar–Ar ages indicate effusive activity at 1.7 Ma for the alto Los Volcanes domes, 1.8 Ma for the Honda Grande Creek dome, and 2.7 Ma for the alto Los Godos (Rueda, 2017). Fission track data in zircon show evidence of volcanic activity between 5.9 and 1.8 Ma based on the average of all grain ages (Bernet et al., 2016).

The volcanic caldera hypothesis (Cepeda & Pardo, 2004) is now discarded because the basal unit (vitreous ignimbrite) actually corresponds to emplacements of the dome structures. Their geomorphology is not due to a caldera collapse but rather to the eruption of two dome complexes (alto Los Volcanes and alto Los Godos) on either side of the Honda Grande Creek valley, which forms a depression between them (Rueda, 2017).

4.2. Structural Geology

The Paipa geothermal area is located in the axial zone of the Eastern Cordillera of Colombia, which has been subject to tectonic inversion and extension since the Cretaceous (Colletta et al., 1990; Cooper et al., 1995; Dengo & Covey, 1993; Fabre, 1983). Velandia (2003) showed that the reactivation of old and new structures is related to the compressive regime during the Andean Orogeny. In the area of interest, there are traces of a transpressive tectonics in the Boyacá and Soapaga Faults. According to Velandia (2003), there are two structural styles in the area (Figure 5). Thick skin style normal faults such as the Cerro Plateado, Paipa–Iza, Las Peñas, and Agua Tibia Faults cut the basement. Thin skin style structures comprise thrust faults in the northwest area that include El Bizcocho, El Batán, El Hornito, Canocas, Santa Rita, El Tuno, Rancho Grande, and Buenavista Faults. All of them are reverse type structures.

The steep subvertical faults (e.g., Paipa–Iza and Cerro Plateado) provide permeability for hydrothermal circulation and magma ascent. Stratigraphic units (Plaeners Formation) and fault intersections also form channels for fluid flow (Velandia, 2003).

4.3. Hydrothermal Alteration

In the Paipa geothermal area, the surface hydrothermal alteration is mainly related to water–rock interaction involving acidic low temperature waters. Intense acid alteration in El Durazno Intrusive is described by González et al. (2008). X–ray diffraction analyses indicate igneous phases made of sanidine and quartz and hydrothermal minerals made of kaolinite and alunite. The acid hydrothermal alteration extends to shallow
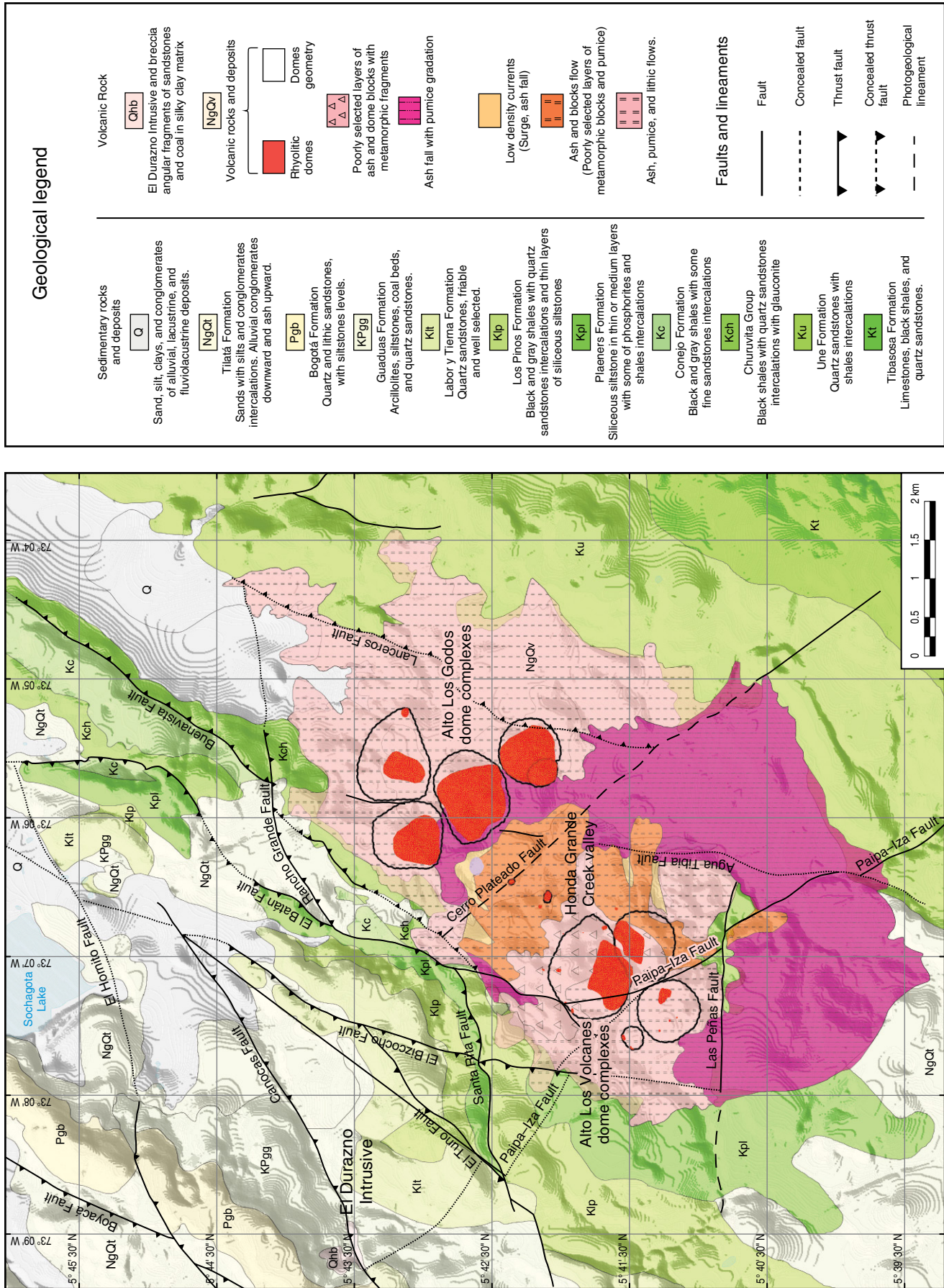
Geological legend

Sedimentary rocks and deposits

Q — Sand, silt, clays, and conglomerates of alluvial, lacustrine, and fluviolacustrine deposits.

NgQt — Tilatá Formation
Sands with silts and conglomerates intercalations. Alluvial conglomerates downward and ash upward.

Pgb — Bogotá Formation
Quartz and lithic sandstones, with siltstones levels.

KPgg — Guaduas Formation
Arcillolites, siltstones, coal beds, and quartz sandstones.

Klt — Labor y Tierna Formation
Quartz sandstones, friable and well selected.

Klp — Los Pinos Formation
Black and gray shales with quartz sandstones intercalations and thin layers of siliceous siltstones.

Kpl — Plaeners Formation
Siliceous siltstone in thin or medium layers with some of phosphorites and shales intercalations.

Kc — Conejo Formation
Black and gray shales with some fine sandstones intercalations.

Kch — Churuvita Group
Black shales with quartz sandstones intercalations with glauconite.

Ku — Une Formation
Quartz sandstones with shales intercalations.

Kt — Tibasosa Formation
Limestones, black shales, and quartz sandstones.

Volcanic Rock

Qhb — El Durazno Intrusive and breccia angular fragments of sandstones and coal in silky clay matrix

NgQv — Volcanic rocks and deposits

Domes geometry

Rhyolitic domes

Poorly selected layers of ash and dome blocks with metamorphic fragments

Ash fall with pumice gradation

Low density currents (Surge, ash fall)

Ash and blocks flow (Poorly selected layers of metamorphic blocks and pumice)

Ash, pumice, and lithic flows.

Faults and lineaments

Fault

Concealed fault

Thrust fault

Concealed thrust fault

Photogeological lineament

Figure 3. Geological map edited from Velandia (2003), Cepeda & Pardo (2004), and Rueda (2017).
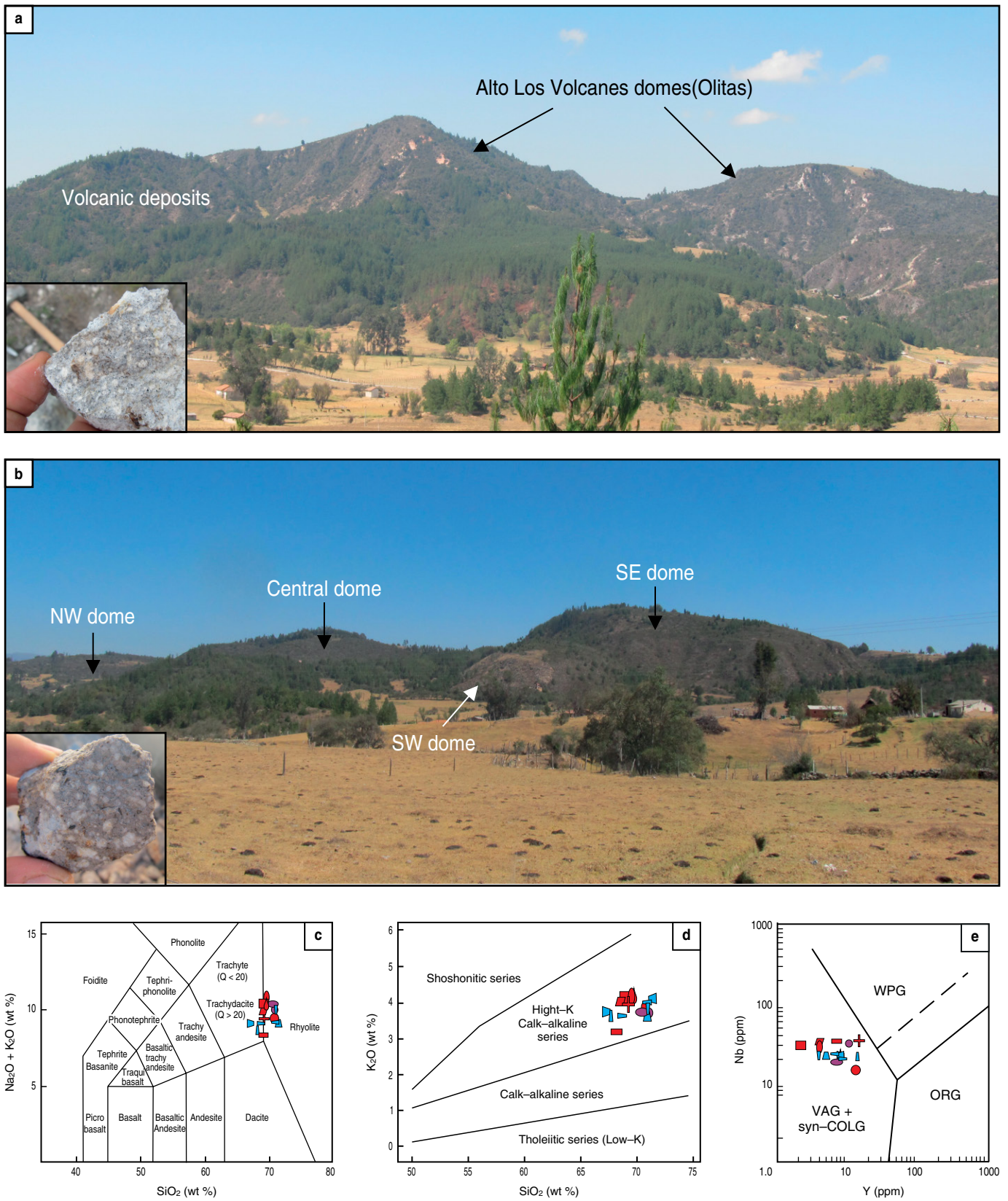
Figure 4. Expression and composition of the dome complex located in the geothermal area. **(a)** Alto Los Volcanes domes. **(b)** Alto Los Godos domes. **(c)** TAS classification of rock composition. **(d)** K$_2$O vs. SiO$_2$ concentrations (Peccerillo & Taylor, 1976). **(e)** Tectonic origin (Pearce et al., 1984). VAG: Volcanic arc granites (Rueda, 2017).

Figure 5. Structural geology of the Paipa geothermal area. **(a)** Regional framework. **(b)** Detailed map of the study area. The red arrows represent the direction of block rotation (Velandia, 2003)

depths (50 and 100 m) in core samples of 4 boreholes (Figure 6), and X–ray diffraction analysis has proven the existence of alunite and kaolinite plus additional secondary minerals such as muscovite, barite, dickite, pyrite, and tridymite (Rodríguez & Alfaro, 2015).

X–ray diffraction of the volcanic deposits characterize oxidation and weathering that overprint hydrothermal alteration. These comprise kaolinite veneer that covers the surface of pyroclastic deposits and hematite–limonite that forms yellow and reddish staining.

Xenoliths in the alto Los Volcanes sector show low intensity, high temperature alteration (Alfaro, 2005a). Some xenoliths comprise sedimentary and rhyolitic clasts in which plagioclase is replaced by epidote and cross cutting veins are filled with chlorite and albite, indicating temperatures exceeding 220 °C (Figure 7a–h). Metamorphic xenoliths containing biotite, adularia, and quartz filled veins suggest hotter alteration temperatures up to 320 °C (Figure 7i–l; Alfaro, 2005a).

4.4. Radiogenic Heat Production

From the concentrations of ^{238}U, ^{232}Th, and ^{40}K measured by gamma spectrometry in core samples from boreholes drilled by SGC at El Durazno Intrusive (González et al., 2008), the average heat production was estimated. The highest concentrations of ^{238}U are found in boreholes 2 and 3, with values of up to 159 mg/kg and 374 mg/kg, respectively. The highest ^{232}Th concentration was measured in borehole 2, with values of 133 ppm. ^{40}K concentrations are similar in boreholes 1, 3, and 4, with concentrations up to 7%, but in borehole 2, the ^{40}K concentration is significantly lower (up to 1.16%) (Rodríguez & Alfaro, 2015).

The radiogenic heat contribution of the boreholes was estimated using equation 1 (Beardsmore & Cull, 2001), which establishes that the radiogenic heat rate generated is related to radioactive decay rate and particle emission energy:

$$A = \text{abundance in the rock (ppm of } ^{238}\text{U}, \, ^{232}\text{Th or} \\ \%^{40}\text{K)} \times \varrho \times A'(\mu W/kg),$$
$$(\text{Equation 1})$$

where A is the rate of heat generation, ϱ the density of the rock, and A' is the constant of heat generated by the decay of ^{238}U, ^{232}Th, and ^{40}K.

The results are scattered, and, for that reason, the box diagram was used to represent these data (Figure 8). Borehole 2 has the highest average heat generation, with a value of 12.52 μWm^{-3}, which is of the same order of magnitude as that for the Copper Basin intrusion (10.3 μWm^{-3}) (Middleton, 1979). However, although the dimensions of El Durazno Intrusive are unknown at depth, it is clearly much smaller.

4.5. Fluid Geochemistry

The Paipa geothermal area is characterized by abundant water and gas discharges from hot springs (Figure 9); the summary that follows of the geochemistry and isotope composition of hydrothermal fluids is based on Alfaro (2002a, 2002b, 2005b). These manifestations are distributed in two main discharge zones: the ITP–Lanceros and La Playa sectors. The ITP–Lanceros sector is located near the intersection of El Bizcocho and El Hornito Faults in Quaternary deposits, and this area has the largest number of hot springs and the highest flow rates. The most representative of these is Pozo Azul, which is 56 °C and flows at 6 L/s (Fonseca, 2018). In La Playa sector, approximately 3.5 km to the south of the main discharge zone in the Plaeners Formation, there are fewer springs, but they have the highest temperatures, which are up to 76 °C; there is a low–pressure steam vent at 75 °C.

The Salpa springs (named after a salt plant) have temperatures of 21 °C and coincide with the Quaternary deposits northeast of the ITP–Lanceros sector. El Hervidero spring is a bubbling intermittent spring, which at 21 °C emerges through deposits 1.5 km south of La Playa. The Olitas spring (23 °C) is located in the alto Los Volcanes dome complex. The pH of most waters is neutral, and the high TDS of the ITP–Lanceros, La Playa, and Salpa buffers the pH. The exception is El Hervidero spring, which is moderately acidic at pH = 3.7 (Table 1).

According to their chemical classification (Figure 10a), the dominant thermal water type, including those from ITP–Lanceros, La Playa, and Salpa springs, is sodium sulfate, with high salinity (20 000 to 60 000 mg/l of total dissolved solids). El Hervidero and Olitas are low salinity springs (<150 mg/l of total dissolved solids) and are classified as sodium sulfate and sodium bicarbonate types, respectively.

The pattern of dissolved species of Salpa springs is similar to that for the hot springs in the ITP–Lanceros and La Playa sectors (Figure 10b). The evidence of a mixing process is confirmed by linear trends in the Na–K–Mg diagram (Figure 11a) and the stable isotope plots (Figure 11b). The highest temperature spring (El Batán) is the least affected by mixing.

The isotope composition of El Hervidero deviates from the mixing trend (Figure 11b) and shows a very significant oxygen–18 depletion that is possibly due to the ^{18}O fractionation between CO_2 and H_2O (Bertrami et al., 1992).

The highest oxygen–18 content corresponds to the Salpa springs, and there is a direct correlation between sodium sulfate concentration and ^{18}O enrichment. This results not from high temperature water–rock interaction but mixing (Alfaro, 2002b). The end–member meteoric water composition is δD –75‰ and δ^{18}O –11‰. The estimated recharge elevation is approximately 2800–2900 masl. From this, and considering that the Une Formation has good permeability, the Tibasosa–Toledo Anticline,

Quaternary

Borehole–1

Borehole–1	Depth (m)	Sanidine %	Quartz %	Alunite %	Muscovite %	Kaolinite %	Barite %	Dickite %	Pyrite %
P1–1	12	61.1	18.1	12	<2	8.5			
P1–2	23	70.5	11.5		10.5		2.7	4.8	
P1–3	32	7.7	80.9		9.1		2.3		
P1–4	40	3.3	80.2		5.9	8.5	2.1		
P1–5	50	17.1	11.3		35.7	24.7			9.4
P1–6	60	31.9			34.5			17.4	16.1
P1–7	85	16.9	27.9	7.4		16.9	4.4		11.6
P1–8	95	5.7	31		<2	8.2			9
P1–9	100	17.5	31		18.3	13.6	3.9		9.7

Borehole–2

Borehole–2	Depth (m)	Sanidine %	Quartz %	Alunite %	Muscovite %	Kaolinite %	Barite %	Pyrite %	Tridymite %
P2–1	1	54.9	28.7	2.7	12.3				
P2–2	12	45	39.4	4.1	8.8				
P2–3	23		25.1	56.9				4.2	
P2–4	32		56	30.5			10.9	2.5	
P2–5	40		4.9	7.8			9.4	8.8	
P2–6	50		7.6	51.3		7		14.6	
P2–7	60		50.9	20		12.9	<2	4	
P2–8	85		47.5	3.6		2		7.6	37.8
P2–9	95		61.3			2.2	4.6	6.1	3.5
P2–10	100		14.1	4.7		8.8	14.7	10.4	43.5

Borehole–3

Borehole–3	Depth (m)	Sanidine %	Quartz %	Pyrite %	Muscovite %	Barite %	Dickite %	Orthoclase %
P3–1	7	18.6	60.3	7.9	14.7			
P3–2	14	71.1	21.6	5.8	5.9		<2	
P3–3	21	65.2	29	3.1	5.5			
P3–4	28	57.9	31.7	3.5				
P3–5	35	46.7	36.1	6.4	5	<2		3
P3–6	42	54.1	27.4		4.9	5.2	2.2	
P3–7	49	<2	27.6		2.1	<2	<2	62.6
P3–8	56	<2	15.1		4.1	<2	8.8	72.9

Borehole–4

Borehole–4	Depth (m)	Sanidine %	Quartz %	Alunite %	Muscovite %	Dickite %	Orthoclase %
P4–1	6	62.8	9.5	6	17.5	2.4	
P4–2	12	88.9		3.3	3.9		
P4–3	18	63.1	13.4				
P4–4	24	52.3	43.3		3.5		
P4–5	30	82.6	11.2		5.7		
P4–6	36	2.5	48.3				48.2
P4–7	42	67.3	<2	20.3		8.2	
P4–8	48		44.5	26.8			26.3

Figure 6. Cores samples from boreholes drilled in El Durazno Intrusive. The mineral composition was determined from XRD analyses (Rodríguez & Alfaro, 2015).
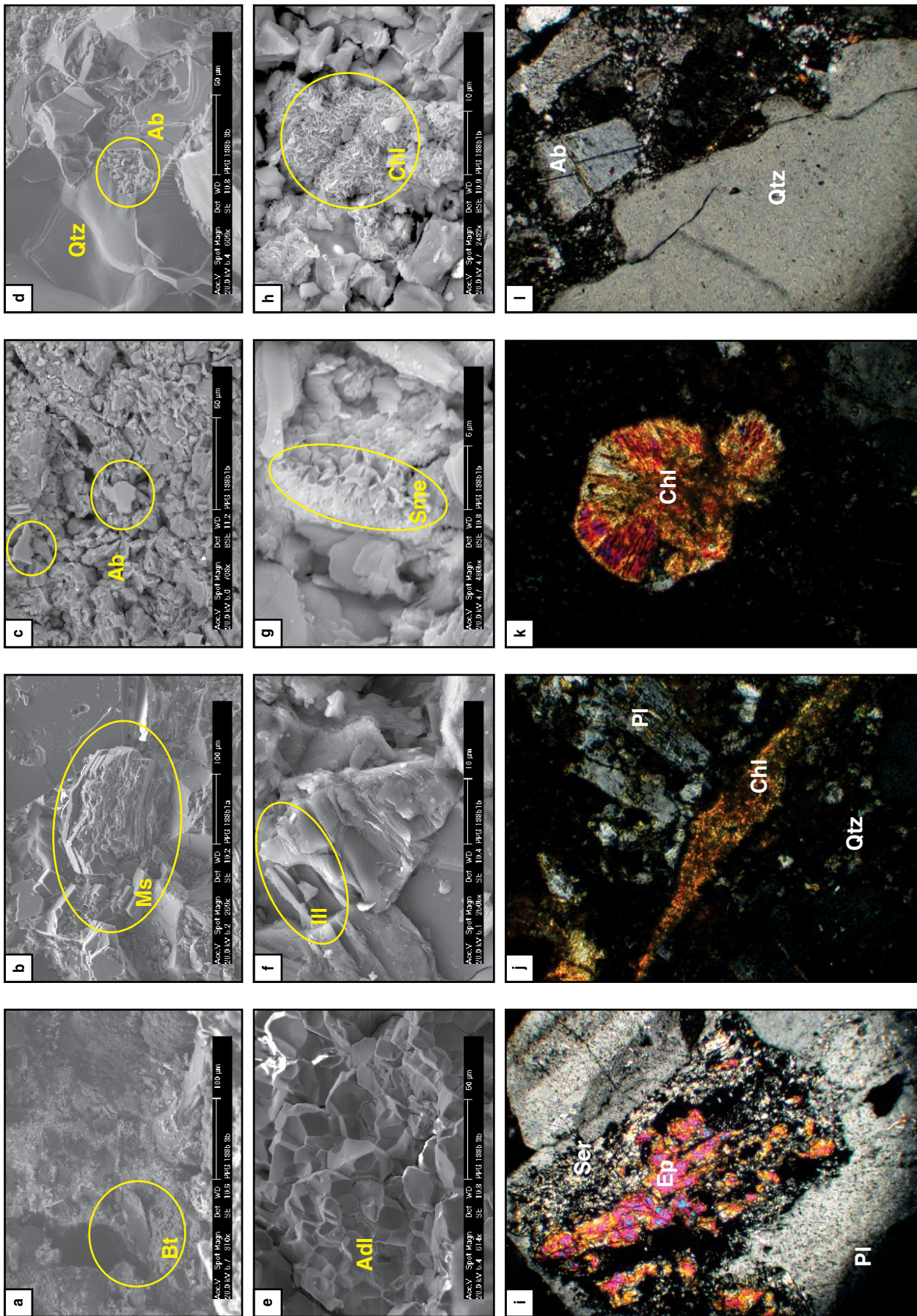
Figure 7. Secondary minerals identified in xenoliths and scanning electron microscopy images of vein filling minerals. **(a)** (Bt) Biotite. **(b)** (Ms) Muscovite. **(c)** (Ab) Albite. **(d)**. (Qtz) Quartz. **(e)** (Adl) Adularia. **(f)** (Ill) Illite. **(g)** (Sme) Smectite. **(h)** (Chl) Chlorite. Petrography in xenoliths in alto Los Volcanes. **(i)** (Ep) Epidote replacing (Pl) Plagioclase and (Ser) Sericite. **(j)** (Chl) Chlorite in quartz vein. **(k)** Radial (Chl) Chlorite replacing feldspathic matrix. **(l)** (Ab) Albite in veins. Figure 7i–l in crossed nicols (Alfaro, 2005a).
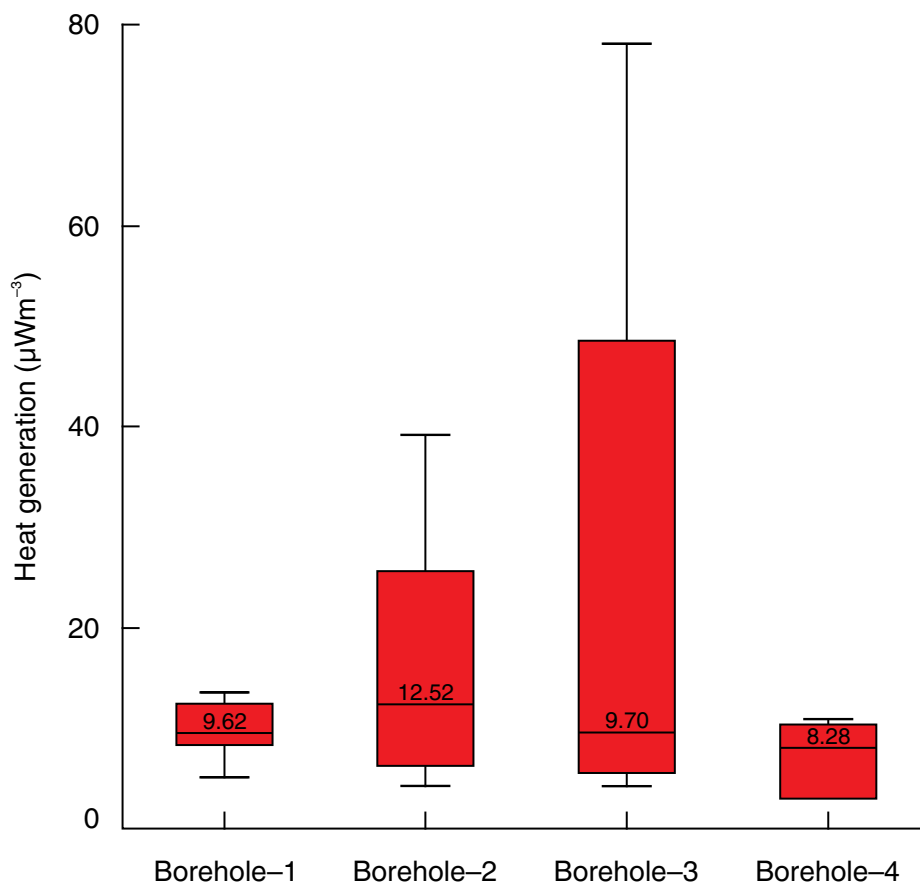
Figure 8. Box diagram representing the estimated heat production for boreholes drilled at El Durazno Intrusive (Rodríguez & Alfaro, 2015).

located east of the study area, is likely the main recharge zone (Alfaro, 2012; Malo & Alfaro, 2017).

Hot springs in ITP–Lanceros and springs in Salpa and El Hervidero are characterized by continuous strong gas discharge. The gas composition of some springs (Table 2) is dominated by CO_2, with a lower CH_4 concentration than expected for geothermal fluids ($CH_4/CO_2 < 0.0001$) (Figure 12a), which could be related to the input of low methane magmatic gas or to oxidizing environments associated with protracted interaction with aerated groundwater. The $\delta^{13}C_{CO2}$ ranges between –4.7 and –4.9‰ in ITP–Lanceros hot springs, and it is –6.7‰ in Salpa and –3.1‰ in El Hervidero. From this, the most likely source of the CO_2 is magmatic given that the mantle–derived values are –5 to –7‰ (Hoefs, 1978). The variation of $\delta^{13}C_{CH4}$ versus $\delta^{13}C_{CO2}$ (Figure 12b) found in the Pozo Inundado spring from the ITP–Lanceros sector and El Hervidero shows that the origin of CO_2 is magmatic and characteristic of geothermal gases which ranges between –2 and –9‰ (Ono et al., 1993). $^{13}C_{CH4}$ ranges from –35.85 and –33.49‰; it does not reflect the typical geothermal gases, for which the range is between –30 to –24‰ (Ono et al., 1993). This composition could be due to the contribution of thermogenic methane,

which is the component of natural gas in which the $\delta^{13}C_{CH4}$ values range from –25 to –55‰ (Schoell, 1980). This suggests that gases of two different origins have mixed (Alfaro, 2005b). Based on recent results for $^3He/^4He$ and $^4He/^{20}Ne$, the contribution from a mantle source is estimated to be between 35 to 55% (Figure 13).

Aqueous and gas geothermometers seem to be unreliable due to the lack of equilibrated deep fluid in hot spring discharges. The alkali geothermometers are not applicable, as the contribution of the saline source is dominant, which is evident in the triangular Na–K–Mg plot (Figure 11a). The source of elevated concentrations of sodium, sulfate, and other ions species are likely due the dissolution of an evaporite deposit. The SiO_2 geothermometers indicate temperatures up to 120 °C (Table 3), and using a simple enthalpy–silica model (Truesdell & Fournier, 1977), the highest possible equilibration temperature is close to 230 °C.

The results of the calculation of geothermometers based on chemical composition and ^{13}C in CH_4/CO_2 are shown in Table 3. The calculated equilibration temperatures range widely between 41–92 °C (CO_2/H_2 geothermometer) to 340–522 °C (CH_4/CO_2 geothermometer) and none of them seem reliable.
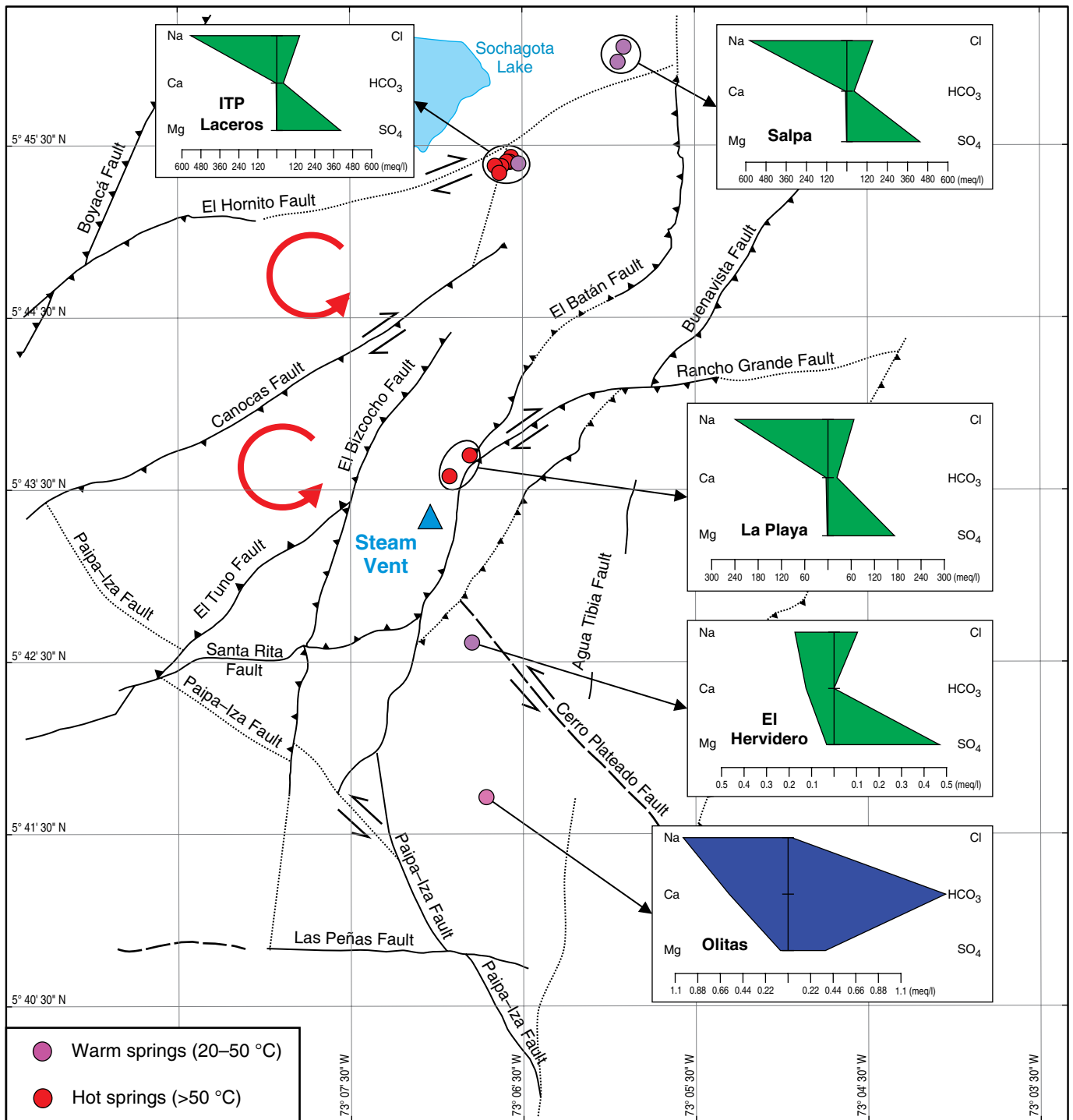
Figure 9. Locations of hot springs. The Stiff diagrams show the predominance of sodium sulfate waters (Alfaro, 2002a).

4.6. Shallow Temperature Survey

A shallow temperature survey was conducted in the Paipa geothermal area. A total of 141 temperature measurements were recorded at the surface and to 20 and 150 cm depths away from the immediate zones of influence of the hot springs (Rodríguez & Vallejo, 2013). The measurements were normalized by subtracting the average ambient temperature, and the results are presented in Figure 14.

The average normalized temperature is 4.9 °C. Two positive anomalies (8.4 and 8.6 °C), well–defined by data, are observed, they occur around the intersection of El Bizcocho, Santa Rita, El Tuno, Paipa–Iza, and El Batán Faults, and another in the corridor bounded by El Hornito and Canocas Faults. In the same

Table 1. Chemical and isotopic composition of hot springs from the Paipa geothermal system (Alfaro, 2002a, 2002b).

ID	Hot Spring	T °C	pH	Electrical conductivity (mS/cm)	Na	K	Ca	Mg	Li	Sr	B	Fe	Mn	Cl	SO$_4$	HCO$_3$	F	Si	SiO$_2$	S Cationes	S Aniones	TDS	d^{18}O	dD
											Concentration (mg/l)												(‰) V–SMOW	
											ITP–Lanceros													
1	Pozo Azul	53.7	7.0	44500	13525	1500	90	18.0	18	4.8	5.20	0.3	1.8	5351	20187	2700	15.2	30	64	632.51	616.57	38652	–6.935	–67.05
2	Pozo Inundado	43.5	7.3	41400	11750	1400	77	17.0	18	4.4	5.30	0.4	1.5	4890	19687	2475	14	27	58	552.03	589.40	36094	–7.025	–66.5
3	Manantial Pozo Inundado	52.7	6.8	42900	12250	1500	77	18.0	18	4.6	4.80	0.4	1.7	5253	19750	2580	14.8	29	62	576.42	602.71	38024	–7.035	–68.15
4	Pozo H. Lanceros	63.4	7.2	42500	12500	1400	87	17.0	18	4.6	4.90	0.3	1.7	5138	19375	2520	14.7	30	64	585.14	590.67	36680	–7.46	–70.15
5	Ojo del Diablo	68.1	7.0	43200	12375	1562	175	21.2	18.2	5.7	5.10	0.2	1.6	5103	19250	2606	15.5	31.5	67.5	588.61	588.53	38848	–7.205	–68.2
6	Pozo Blanco	62.2	7.0	44100	13000	1500	100	17.0	20	4.6	4.90	0.4	1.8	5333	20937	2640	15.3	30	64	610.10	630.71	38218	–7.215	–67.9
7	Cuarto Máquinas Tobogan ITP	22.9	6.0	8320	1550	160	40	8.0	1.6	0.4	0.05	<0.2	<0.1	728	2870	298	0.48	7	15	74.16	85.24	5004	–9.56	–71.55
8	Fondo piscina olimpica	25.1	6.0	11130	2450	280	48	10.0	3.4	0.6	0.09	<0.2	0.6	1154	4187	479	0.29	7	15	116.93	127.65	8042	–9.365	–70.2
9	Fondo piscina olimpica	30.2	6.3	27600	6883	810	100	20.0	10	1.6	2.10	<0.2	2.9	3009	13062	1402	1.4	10	21	326.70	380.06	21344	–8.49	–70.45
10	Fondo piscina olimpica	25.9	6.1	9750	1975	230	50	10.0	2.2	0.4	0.60	<0.2	<0.1	985	3050	373	0.13	6	13	95.10	97.45	6922	–9.475	–71.5
11	Motobomba Lanceros	69.8	7.1	43300	12375	1550	175	22.5	18.1	5.8	5.10	0.3	1.6	5065	19812	2606	15.30	30.0	64.3	588.41	599.15	38750	–7.335	–69.05
											La Playa													
12	El Batán–Piscina La Playa	75.5	7.4	22000	5500	725	100	22.5	10.6	2.4	2.40	<0.2	0.2	2378	8250	1420	18.7	36.0	77.1	264.60	263.22	13500	–8.62	–68.95
13	Vía Escuela La Playa	53.5	6.8	52300	5500	685	40	20.0	10	1.8	6.00	<0.2	0.2	6807	8750	2699	20	35	75	260.36	419.61	41813	–6.685	–67.6
											Salpa													
14	Pozo Las Marismas Salpa	21.5	6.3	55800	16926	1757	47.3	14.6	22.9	5.2	7.40	4.67	2.00	7095	26652	2989	5.76		31.6	784.55	804.69	63664	–6.36	–67.1
15	Pozo principal Salpa	21	6.5	46000	13250	1637	175	22.5	18.0	4.7	5.30	0.2	1.7	5455	20812	2620	6.10	19.5	41.8	628.69	630.73	41612	–7.275	–69.65
											Olitas													
16	Piscina Olitas	23.2	5.7	172.2	23.5	14.5	11.5	0.9	<0.1	0.6	0.03	<0.2	<0.1	1.3	17.5	93.7	3.2	46.0	98.6	2.04	2.11	92	–10.185	–73.35
											El Hervidero													
17	El Hervidero	21.8	3.7	103.2	4.0	5.0	2.5	0.4	<0.1	<0.2	<0.05	1.0	<0.1	3.7	22.5	0.0	0.1	9.0	19.3	0.46	0.58	55	–14.52	–62.9

corridor, a groundwater well of approximately 97 m depth discharges sodium bicarbonate water at 34.8 °C, which is consistent with the temperature anomaly. Negative anomalies (low temperature) occur in the Honda Grande Creek valley, which extends around the alto Los Volcanes dome complexes. This thermal pattern is possibly related to the permeability of the soil, which is lower in the valley, where clay layers from the weathering of pyroclastic deposits form an insulating barrier.

4.7. Vertical Electrical Soundings (VES)

The geoelectrical study, which employed a Schlumberger array and 152 VES, penetrated to a maximum depth of 300 m (Franco, 2016). The survey area is characterized by low (between 12 and 58 Ω·m) and very low resistivities (<12 Ω·m), which is illustrated in three plan maps, at 2500, 2350, and 2200 masl. (Figure 15). The lowest resistivity anomaly is found to the east of Sochagota Lake in the proximity of the Salpa sector, which is the zone of the highest sodium sulfate concentration water (Alfaro, 2002a). An extensive NNW trending anomaly occurs between El Hornito and Canocas Faults (at 2500 masl) and extends to El Tuno Fault at 2200 masl. Other anomalies appear to be controlled by the Cerro Plateado Fault and the corridor between El Batán and Buenavista Faults. At 2350 and 2200 masl, the anomaly related to the Cerro Plateado Fault seems to extend laterally to the
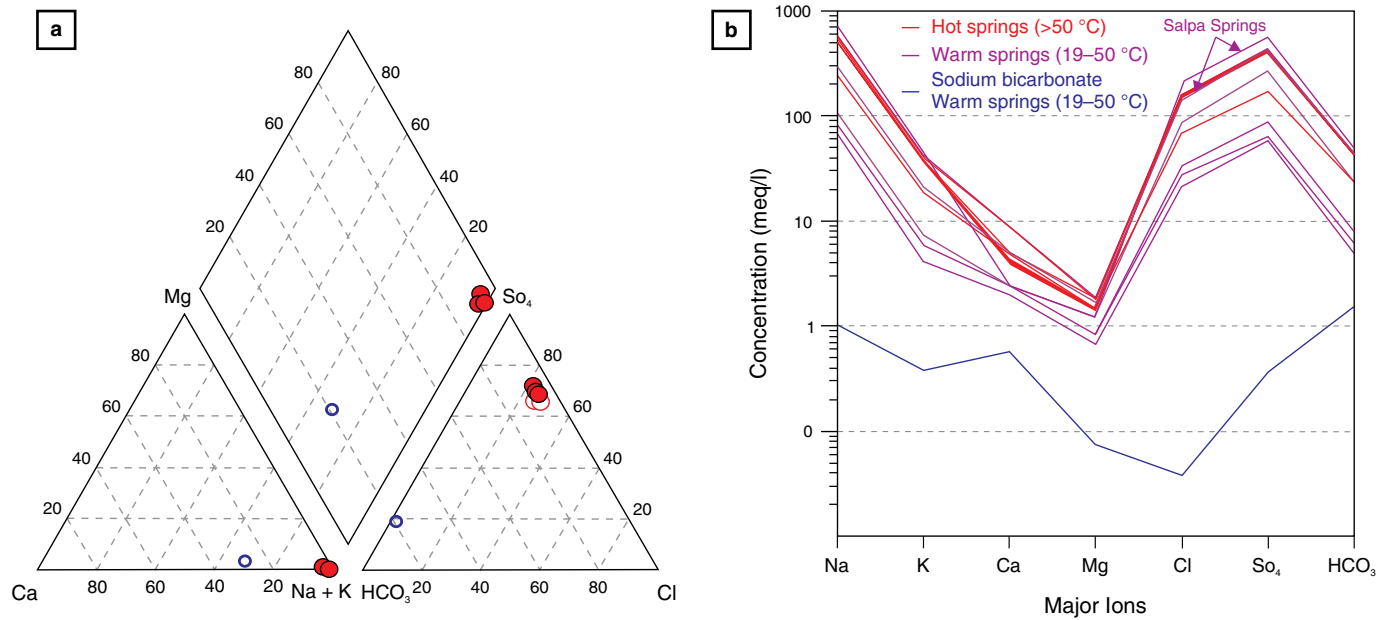
Figure 10. Chemical classification of the spring waters. **(a)** Piper diagram. Most of the springs are of the sodium sulfate water type, except for Olitas spring (blue circle), which is a sodium bicarbonate spring. **(b)** Schoeller diagram. The dominant sodium sulfate pattern followed by the hot springs is clearly defined by the saline springs of Salpa (Alfaro, 2002a).
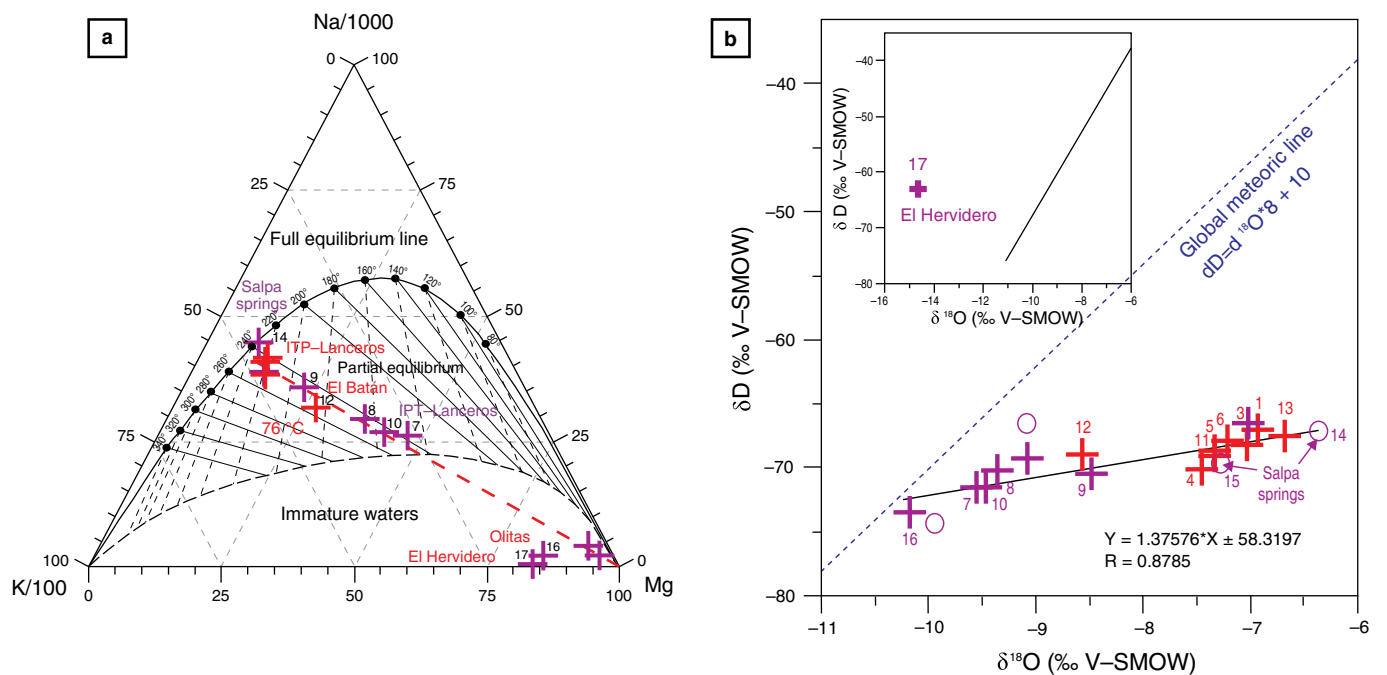

Figure 11. Evidence of a mixing process of hot springs with saline sodium sulfate water. **(a)** Na–K–Mg relative composition (Giggenbach, 1988; Alfaro, 2002a). **(b)** Environmental stable isotopes (Alfaro, 2002b).

west up to El Tuno Fault and to the east up to the Agua Tibia Fault. The low resistivities could be related to the circulation of saline waters resulting from a high concentration of sodium and sulfate water, to the circulation of hydrothermal waters, or to clay layers in the sedimentary sequence (Franco, 2016).

4.8. Gravity and Magnetic Data

The acquisition of gravity and magnetic data was carried out in three field campaigns compiled by Beltrán (2015). An additional campaign was performed to unify the base stations (data levelling) in order to calculate the gravity fields (Vásquez, 2012). After apply-

Table 2. Chemical and isotopic composition of gases discharged by hot springs in the Paipa geothermal system.

ID	Hot Spring	Concentration (molar percentage in dry gas) % (1)									d¹³C$_{CO2}$ (‰) (1)	d¹³C$_{CH4}$ (‰) (1)	He/Ne (2)	³He/⁴He (R/Ra c) (2)
		CO$_2$	H$_2$S	NH$_3$	He	H$_2$	Ar	O$_2$	N$_2$	CH$_4$				
						ITP–Lanceros								
1	Pozo Azul	97.95	0.208	0.00175		0.00099	0.02159	0.90350	0.90768	0.00298	–4.7		1.12	3.39
2	Pozo Inundado	98.43	0.104	0.00286	0.00007	0.00095	0.02886	0.34299	1.07925	0.00688	–4.7	–35.85		
4	Pozo Lanceros	92.26	0.280	0.00118	0.00030	0.00015	0.06592	1.53176	5.85692	0.00356	–4.9			
5	Ojo del Diablo	99.15	0.354	0.00106	0.00025	0.00132	0.00944	0.00435	0.45406	0.02100	–4.8		3.14	3.32
						Salpa								
14	Pozo La Marismas Salpa	99.73	0.129	0.00071	0.00014	0.00011	0.00191	0.02590	0.11027	0.00259	–6.7		6.76	3.56
						El Hervidero								
17	El Hervidero	99.25	0.136	0.00046	0.00411	0.00015	0.00471	0.02825	0.43606	0.13954	–3.1	–33.49	1125.05	2.73

(1) Alfaro (2005b)

(2) This work. Analyses by the Istituto Nazionale di Geofisica e vulcanologia (INGV), from Italy. Agreement SGC–INGV No. 08, 2018.
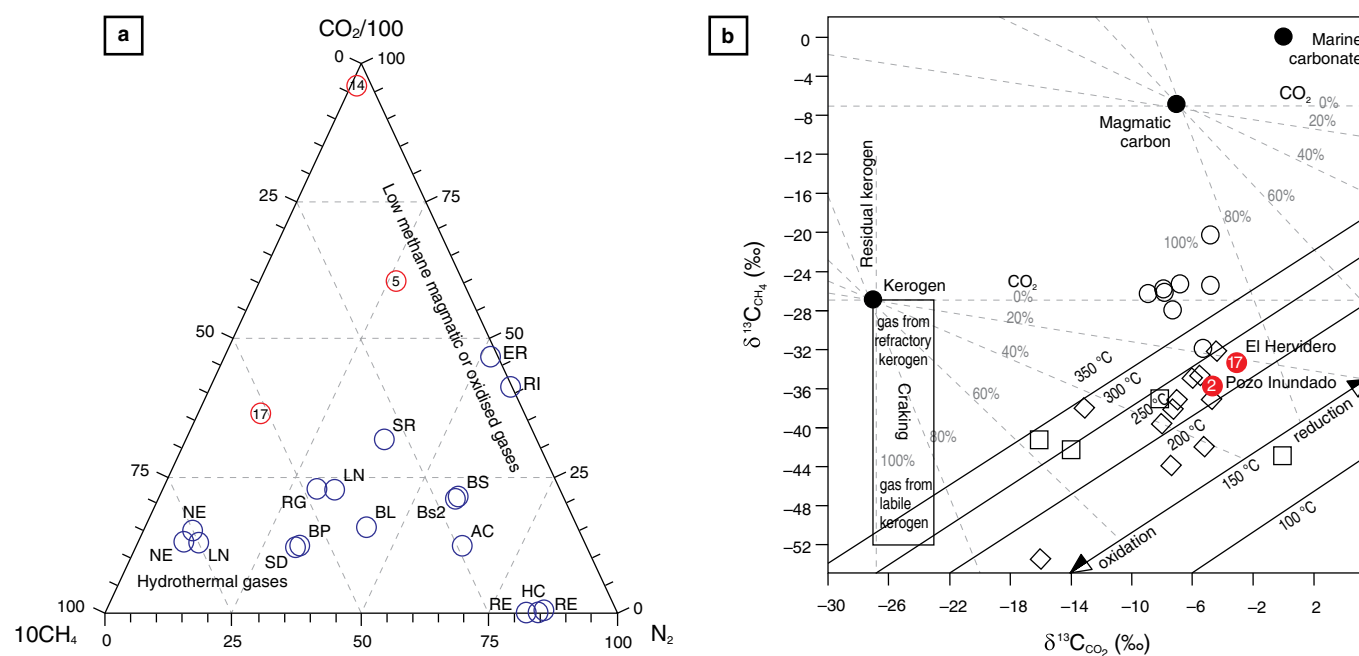
Figure 12. Gas discharge compositions. **(a)** Relative concentrations of CO$_2$–CH$_4$–N$_2$, for which the blue circles correspond to the Nevado del Ruiz as a reference of the typical composition of hydrothermal and magmatic (ER and RI) gases. The red circles 5, 14, and 17 correspond to Ojo del Diablo, Salpa, and El Hervidero hot springs, respectively. Modified from Giggenbach et al. (1990). **(b)** ¹³C$_{CH4}$ vs. ¹³C$_{CO2}$ (Alfaro, 2005b). Circles: geothermal wells from New Zealand. Squares: natural gas wells from New Zealand and Thailand. Diamonds: natural gas wells in the Gulf of Thailand. Modified from Giggenbach (1997).

ing variable density gridding, adjusting the reduction of data, and calculating the power spectrum, the residual anomaly grids were obtained by the application of a matched filter over the total Bouguer anomaly and over the total field magnetic anomaly (Llanos et al., 2015).

The residual gravity map (Figure 16) shows several highs associated with the Paipa Volcano and Las Peñas and Santa Rita Faults; other gravity anomalies are associated with alto Los Godos, which are controlled by the Cerro Plateado Fault.
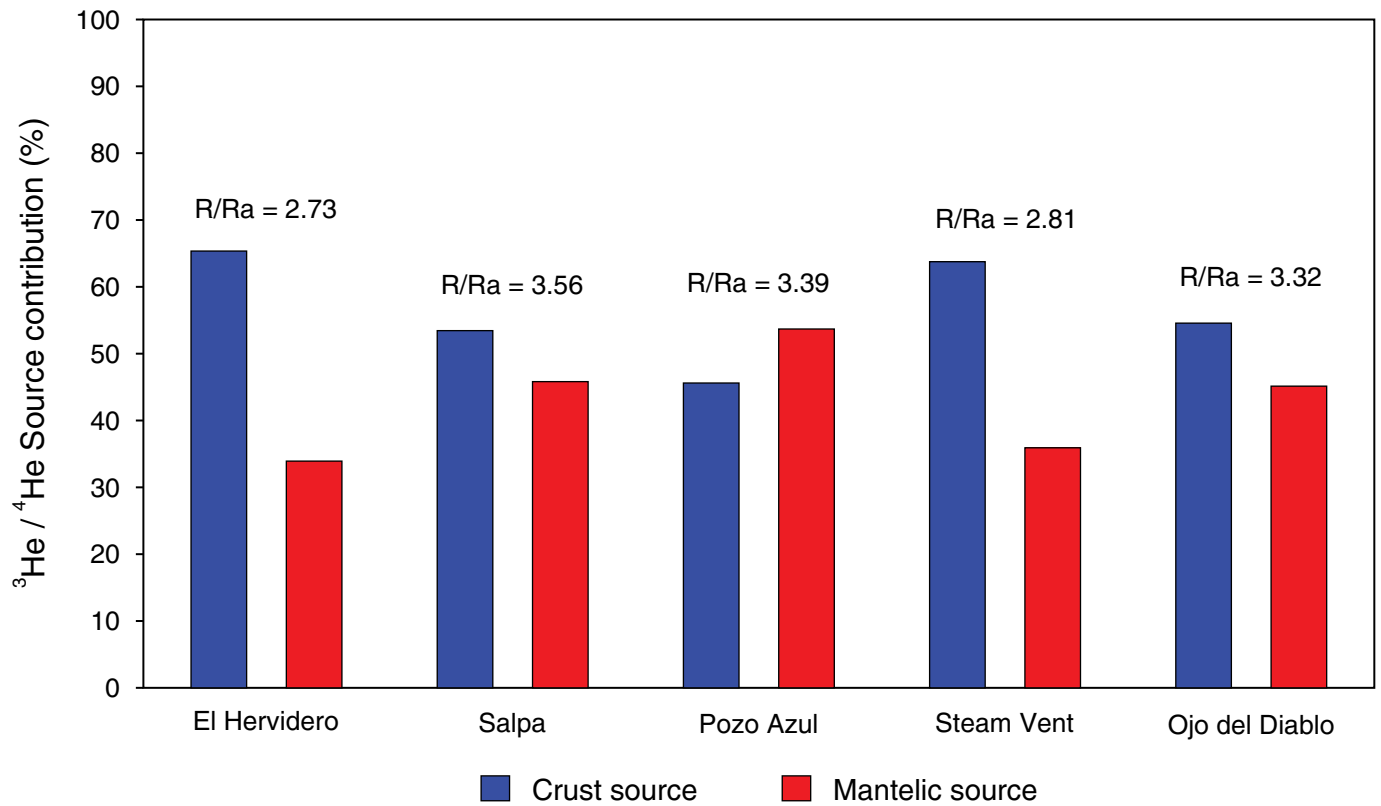
Figure 13. ^{3}He/^{4}He ratios indicating a mantle contribution to the gas compositions.

Table 3. Temperature estimation of the reservoir fluid at Paipa's geothermal system (Alfaro, 2002a, 2005b).

ID	Hot Spring	Sector	Discharge Temperature (°C)	T_{Qtz} –no steam loss	$T_{CH4/CO2}$ °C	$T_{CO2-H2S-H2-CH4}$ °C	$T_{H2/Ar}$ °C	$T_{CO2/Ar}$ °C	$T_{CO2/H2}$ °C	$Td^{13}_{CH4/CO2}$ °C		
				(1)	(2)	(3)	(4)	(5)	(6)	(7)	(8)	(9)
					ITP–Lanceros								
1	Pozo Azul	ITP–Lanceros	54	114	513	108			85			
2	Pozo Inundado	ITP–Lanceros	43	109	468	98			84	220	226	159
4	Pozo Lanceros	ITP–Lanceros	63	114	500	83			43			
5	Ojo del Diablo	ITP–Lanceros	68	117	415	106	116	285	92			
					La Playa								
12	El Batán	La Playa	76	123								
					Salpa								
14	Pozo La Marismas Salpa	Salpa	22		522	74		335	34			
					El Hervidero								
17	El Hervidero		22		340	62	79	305	41	228	233	166

(1) Fournier (1977)

(2) Giggenbach (1991)

(3) D'Amore & Panichi (1980)

(4) Giggenbach (1987)

(5) Giggenbach & Goguel (1989)

(6) Koga (1987) in Koga (2000)

(8) Panichi & Gonfiantini (1978)

(7) Lyon & Hulston (1984)

(9) D'Amore & Panichi (1987)
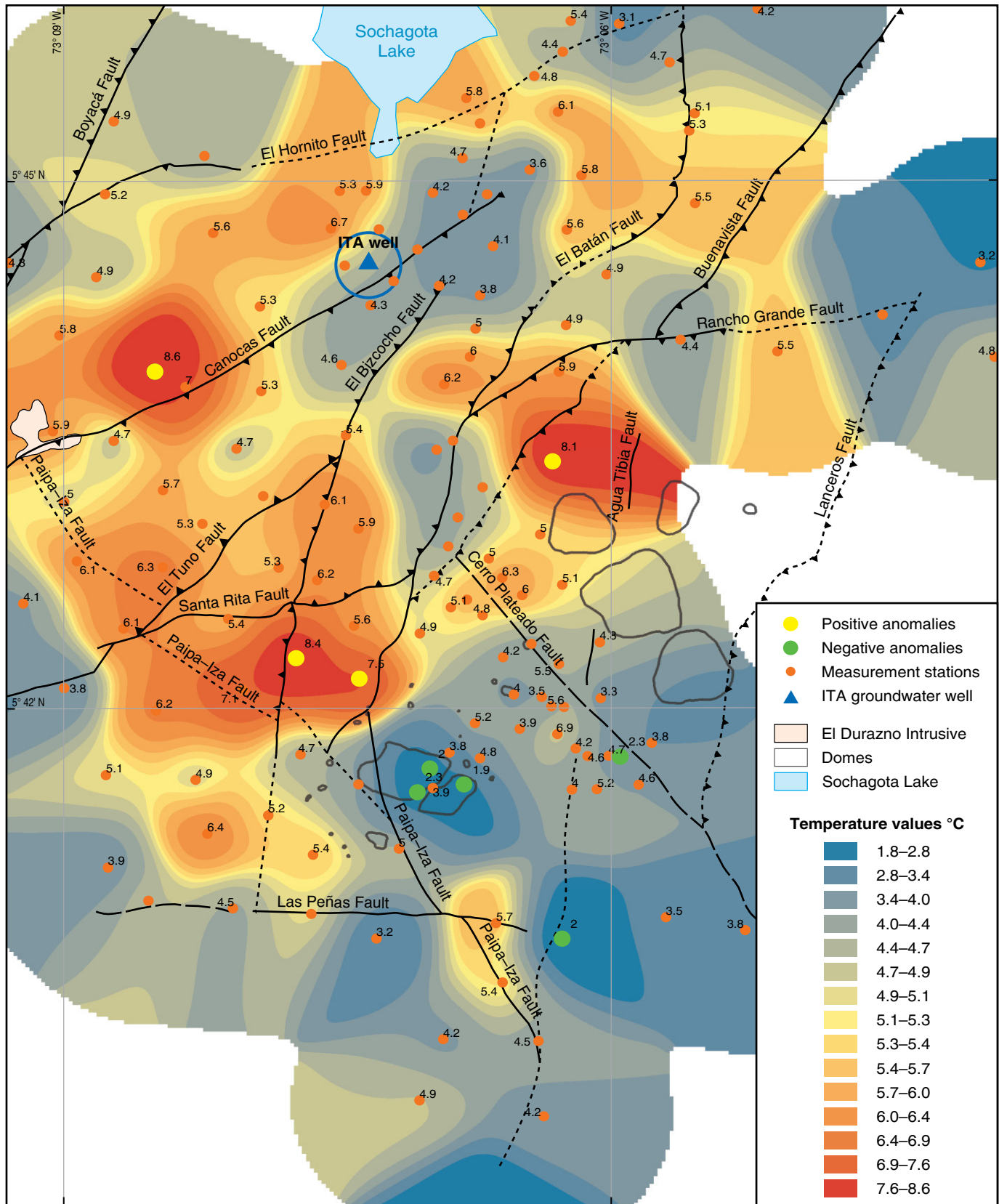
Figure 14. Map of shallow temperatures at 150 cm depth (Rodríguez & Vallejo, 2013).
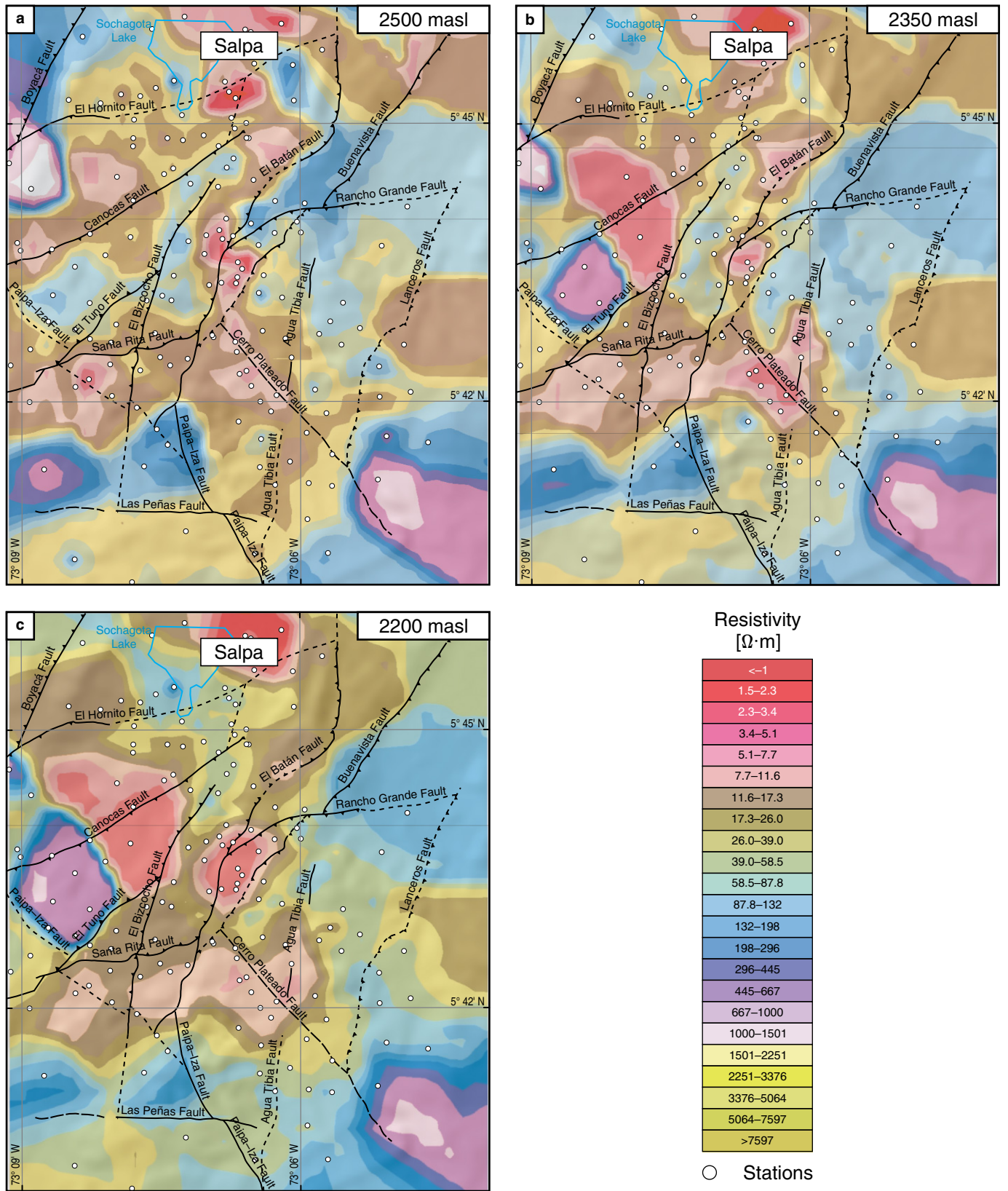
Figure 15. Resistivity maps at **(a)** 2500, **(b)** 2350, and **(c)** 2200 masl (Franco, 2016).
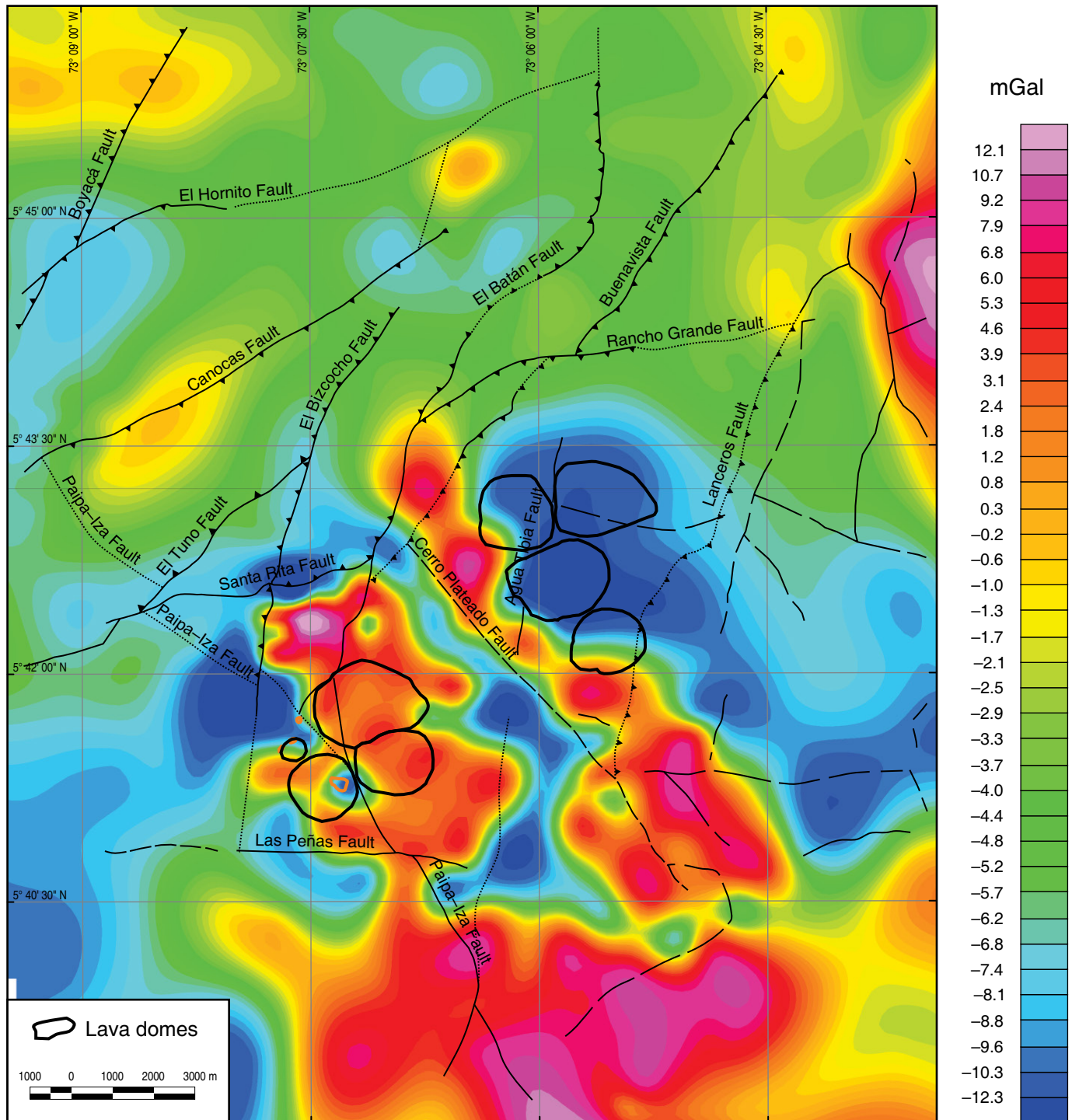
Figure 16. Residual gravity anomaly map. The red color represents gravity highs, and the blue color represents gravity lows (Llanos et al., 2015).

To the south of the Paipa geothermal area, there is another gravity anomaly that could be associated with an intrusive body that lacks surface expression. Westward, in El Durazno Intrusive, intermediate values of gravity are observed. To the northeast, a gravity high is possibly associated with metamorphic rocks from the Floresta Massif or igneous intrusions exposed at the surface north of the geothermal area.

The total magnetic intensity map (Figure 17; Llanos et al., 2015) shows a magnetic high associated with the Paipa Volcano, which resembles the shape of the gravity anomaly and seems to also be controlled by Las Peñas and Santa
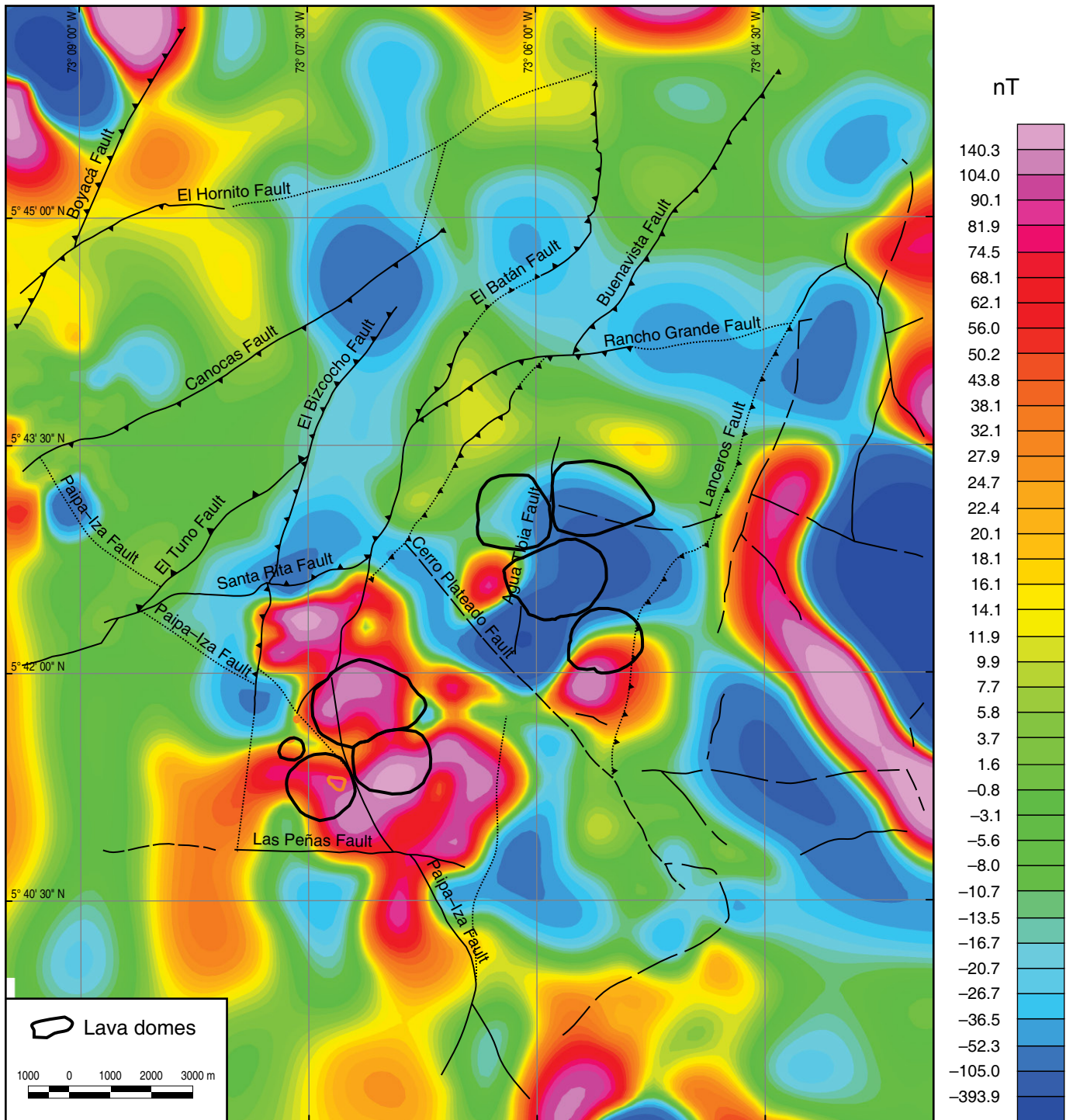
Figure 17. Total intensity magnetic map (Llanos et al., 2015).

Rita Faults. An asymmetric magnetic dipole is associated with the alto Los Godos dome complex. The two highest magnetic anomalies, located in the northwest and east of the area, are interpreted as intrusive bodies (Llanos et al., 2015). To the south, a small dipole possibly reflects a concealed intrusion.

4.9. 3D Geological Model Constrained by Geophysics of Potential Fields

A geological–geophysical 3D model was obtained using Geomodeller inversion software. The input data comprise geological maps from Velandia (2003) and Cepeda & Pardo (2004),

cross sections drawn from the 1:25 000 geological map and gravity and magnetometry grids. After the physical properties (density and magnetic susceptibility) were assigned to each geological formation, a joint stochastic inversion was executed at a voxel resolution of 100 m × 100 m × 100 m (Llanos et al., 2015).

The 3D geological model (Figure 18) contains the sedimentary and metamorphic units, domes (intrusive bodies) and volcanic deposits. The most notable features of the geological model, as constrained by inversion with potential geophysical data, are represented by the 3D density model (Figure 19).

The 3D density model reveals positive anomalies that can be related to attributes of the Paipa geothermal system (Figure 19). Intrusion 1 and 2 underlie the alto Los Volcanes and El Durazno Intrusive, respectively. Intrusions 3 and 4 do not have surface expressions, seem to be related to the alto Los Godos dome complex and are separated from intrusion 1 by the Cerro Plateado Fault. Intrusions 5 and 6 could be related to the high density basement in the Tibasosa–Toledo Anticline or to other blind magmatic intrusions (Alfaro et al., 2017).

4.10. Magnetotelluric Model and Geological Interpretation

Figure 20 shows the locations of five profiles defined for 2D modeling using WinGLink geophysical interpretation software by Geosystem SRL, owned by the SGC (González–Idárraga & Rodríguez–Rodríguez, 2017) and 88 MT soundings used for 3D modeling by means of WSINV3DMT (González–Idárraga & Rodríguez–Rodríguez, 2017). As can be observed in Figure 21, the 2D models and the same profiles from the 3D model visualized using Paraview software show contrasts between very high, intermediate, and very low resistivities, which grosso modo are comparable in the 2D and 3D models. The observed differences are due to the resolving power of 3D anomalies in 2D modeling (Ledo, 2005; Wannamaker, 1999) and due to the projection of anomalies that could appear as "hanging" resistivity bodies in the profiles, which are called phantom anomalies (Ledo, 2005).

Comparing the magnetotelluric 3D model with the density model and bearing in mind some considerations based on surface geology and geological cross sections, a geological interpretation was achieved. Two geological domains are identified as crystalline rocks of high density and high resistivity and sedimentary rocks of comparatively low density and low resistivity.

The sedimentary cover, including volcano–sedimentary deposits, has low to intermediate resistivities between 0 and 80 $\Omega \cdot m$. This cover, presented in Figure 22 in volumetric view generated using Paraview software, is much thicker in the west and northwest, where it reaches 3 to 4 km depth, probably due to the greater accumulation and basin subsidence in the west, when compared to the thinner deposits in the east.

The reported thickness of the Cretaceous to Quaternary sedimentary sequence previously described is approximately 1500 to 2000 m. The Devonian – Carboniferous sedimentary units may comprise almost 1500 m of sand and clay–rich layers. From this, a sedimentary cover of greater than 3000 m thickness can be assumed, which is consistent with the depths of conductive anomalies. Within the sedimentary units, a more conductive layer is identified by resistivities between 0 and 3 $\Omega \cdot m$. This high conductivity is interpreted as the contribution of saline pore waters in permeable intervals, as observed on the surface and in the top 1000 m (Figure 22c).

The geoelectrical response of the basement, shaped by metamorphic rocks intruded by granitic bodies, is resistive, as shown in the volumetric representation of the resistivity presented in Figure 23a. It is located near the surface to the east and southeast and deeper to the west and northwest, where it is below the modeled depth (i.e., >4 km). The most notorious features are the resistive bodies (500–1000 $\Omega \cdot m$) that correlate with the intrusions and high density anomalies (Figure 19) corresponding to El Durazno Intrusive and to the dome zones (Figure 23b). The intrusive structure of El Durazno forms an oval–shaped resistive anomaly that narrows with depth. The extensive high resistivity structure developed beneath the alto Los Volcanes domes extends laterally towards the alto Los Godos domes (Figure 23b); in other words, the same magmatic intrusion fed the two dome complexes, which correlates with the lack of a high density anomaly underneath alto Los Godos (Figure 19). To the east, other resistive structures with shapes and thicknesses similar to those previously described (see the miniatures in Figure 23b) could be due to intrusions with no superficial expression or to rocks from the anticline's nucleus.

4.11. Conceptual Model

The main results of the exploration studies are summarized in Table 4 and Figure 24.

The geothermal system arises and is hosted in terrain that is tilted from south to north towards the Chicamocha River. The recharge occurs at an elevation of 2900 m through the sandstones of the Une Formation in the Tibasosa–Toledo Anticline, which dip towards the west. Once beneath the valley, the groundwater flows downwards, following deep fault structures (Paipa–Iza, Las Peñas, and Agua Tibia Faults) and the intersections between them.

The northward flow through the basement possibly follows secondary permeability channels opened by hydrostatic and hydrodynamic pressure or the contacts along intrusions. Heat is swept by the fluid as a result of the interaction with intrusions beneath the dome complexes' zone. The heat is either related to magmatic activity or is radioactively associated with the decay of ^{238}U, ^{232}Th, and ^{40}K. The geothermal fluid is fed by magmatic
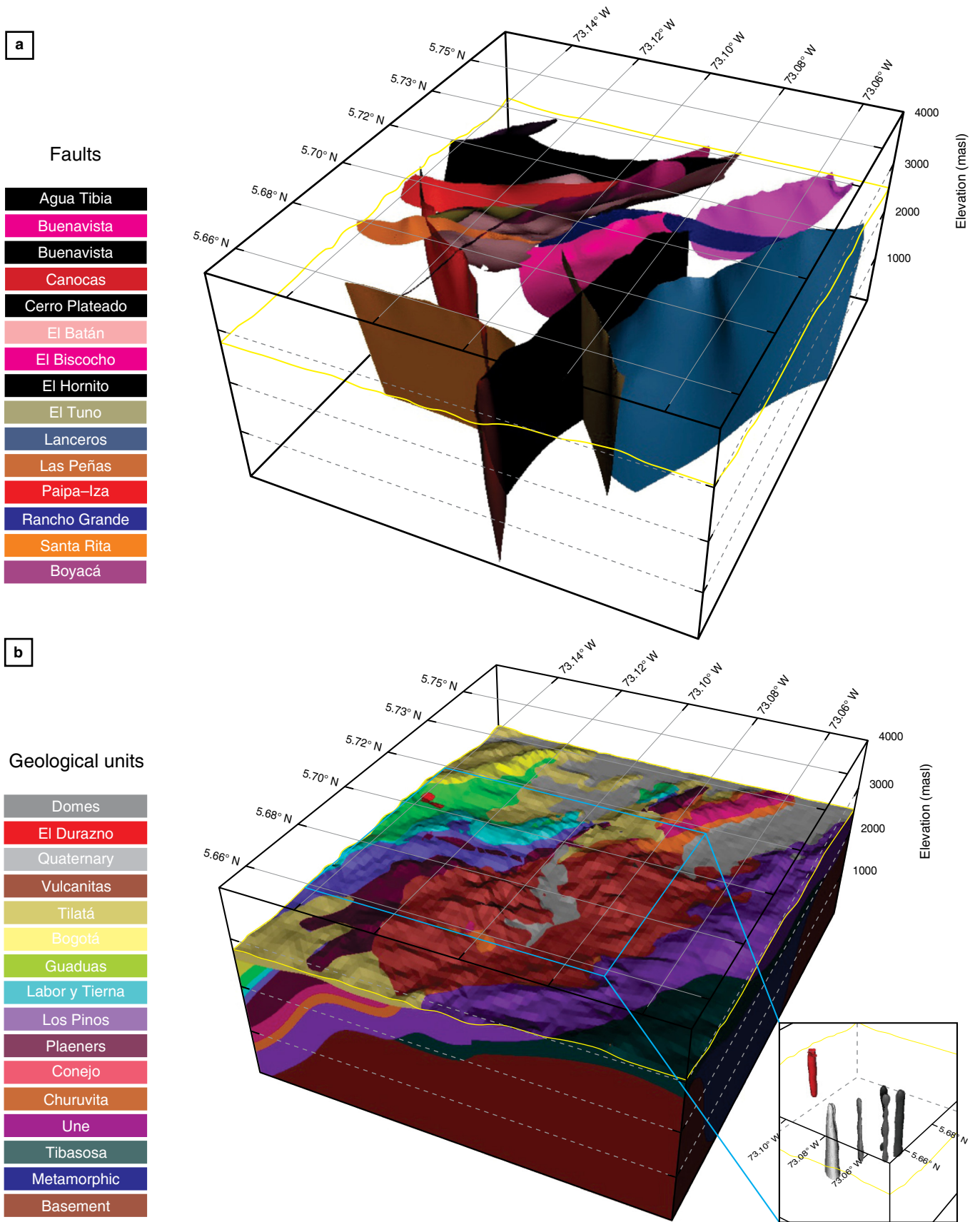
Figure 18. Geological 3D model of the Paipa geothermal area. **(a)** View of the structural model. **(b)** View of the geological model (Llanos et al., 2015).
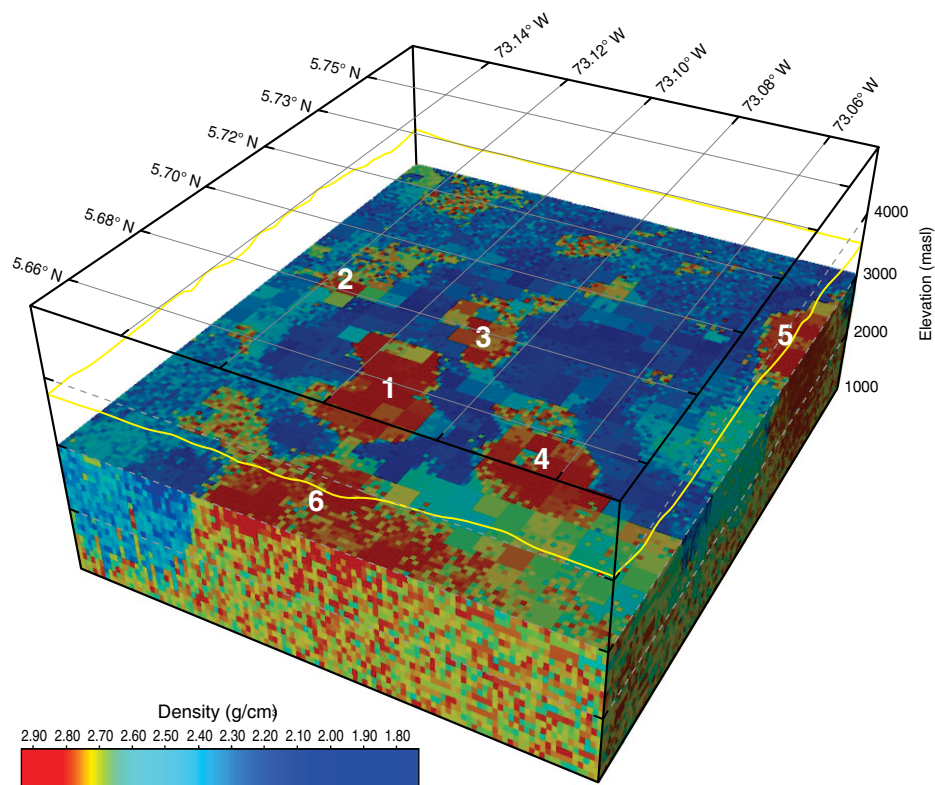
Figure 19. 3D density model of the Paipa geothermal area. The positive anomalies labeled with numbers are related to igneous intrusions (Alfaro et al., 2017).

CO_2 and mantle He ($^3He/^4He$). Due to buoyancy forces, hot water rises along fault controlled conduits (such as the Cerro Plateado Fault) or through porous sedimentary rocks, which creates a sedimentary hosted reservoir.

That low density and intermediate resistivity sedimentary reservoir is hosted in the Une Formation between the two dome complexes. The resistivity related to the sedimentary reservoir and its cap rock does not show a contrast with the sedimentary cover; this electrical response is normal in sedimentary geothermal systems (van Leeuwen, 2016). From this reservoir, the hot water initiates the outflow to the discharge zone following the Cerro Plateado Fault in a NW direction. Along its path, the fluid discharges to the surface in a low permeability zone in hot springs and a steam vent of low flow rate through the Plaeners Formation (La Playa discharge sector). The impermeable clay layers from Churuvita Formation and even from the Une Formation and the weathered pyroclastic deposits would prevent the hot water from flowing to the surface, becoming the cap rock of the system. When the hot water reaches the western limit of the Une Formation, it flows NNE up to the intersection of El Hornito and El Bizcocho Faults to form the main discharge zone (ITP–Lanceros sector).

The chemical and isotopic composition of the hot water is modified by the mixing with the saline pore waters and input of thermogenic methane.

The resistivity structure suggests that the saline source originates to the west due to the partial dissolution of evaporites hosted deep in the sedimentary sequence. The main fluid flow near the surface follows a NE corridor bounded by El Hornito and Canocas Faults up to the vicinity of Sochagota Lake, near the northern border of the area, where it reaches the surface through the Quaternary deposits. At depth, the saline water circulation extends laterally to the east, making possible the mixing process with the geothermal fluid beneath the surface.

At shallow depths in the mentioned NE corridor, warm water feeds the ITA groundwater well and forms a surface thermal anomaly. The low salinity of this well water indicates that the water circuit is separated from the deeper saline water, probably by sedimentary clay layers, which are common in most of the sedimentary sequence. The water would increase its temperature by interaction with igneous intrusive bodies enriched in radiogenic elements, around El Durazno Intrusive or by interaction with warm rocks in contact with the Une Formation, which acts as the conduit of the fluid from the hot geothermal system, as previously described.

5. Conclusions

The Paipa geothermal system was developed in sedimentary stratigraphy of the Eastern Colombian Cordillera. Here, an iso-
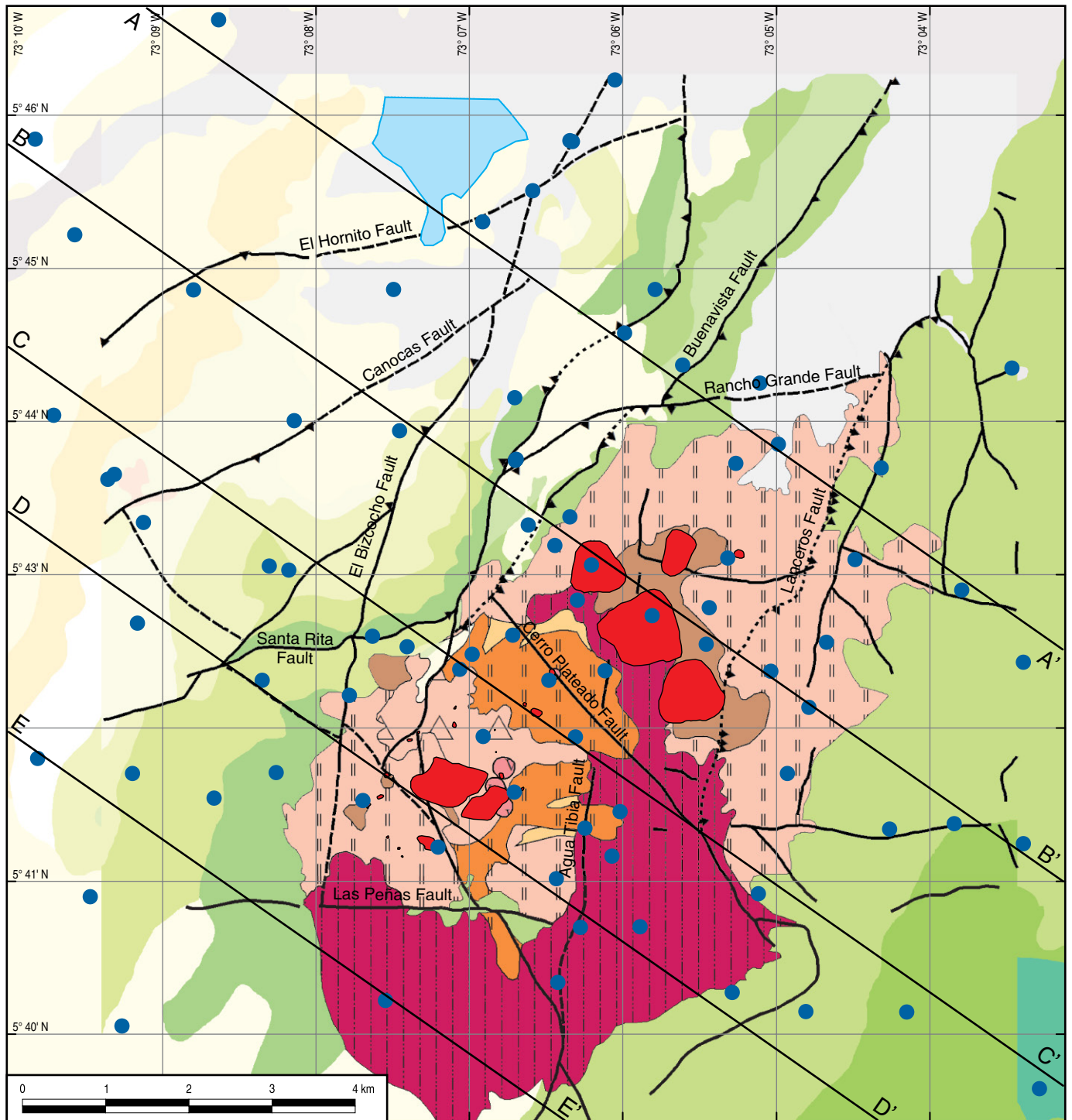
Figure 20. MT survey area showing stations and the locations of 2D profiles. At each sounding, AMT and MT were measured for a range of frequencies of 10^4–0.01 Hz, approximately (Geological map from Cepeda & Pardo, 2004; Rueda, 2017; and Velandia, 2003).

lated volcanic center has been active for the last 1 to 10 Ma, and sodium sulfate–rich groundwaters circulate near the hydrothermal system and mix with the geothermal fluid.

The geological setting is divided into two domains: (1) the thick sedimentary sequence that ranges from the Cretaceous to Quaternary in the west and northwest and, (2) in the central northeast, the developed volcanic intrusive complex with surface expression defined by rhyolitic domes.

The main recharge zone occurs at elevations of 2800–2900 masl, coincident with outcrops of the Une Formation and the Ti-

2D modeling profiles

2D profiles from 3D modeling
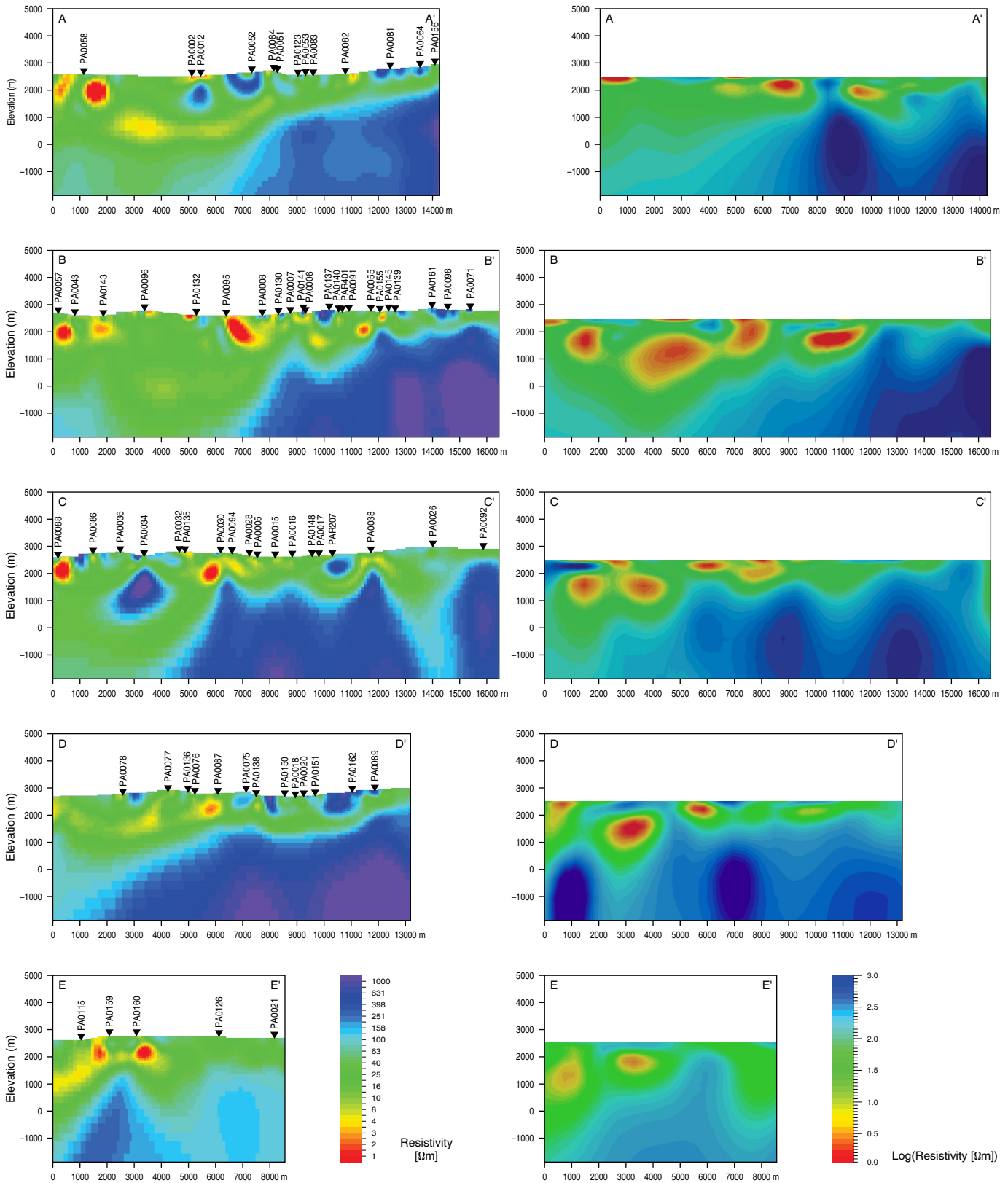
Figure 21. 2D MT profiles. A conductive domain near the surface is observed in the northwest, and a deep resistive domain occurs in the east and southwest of the area from both 2D and 3D modeling (González–Idárraga & Rodríguez–Rodríguez, 2017).
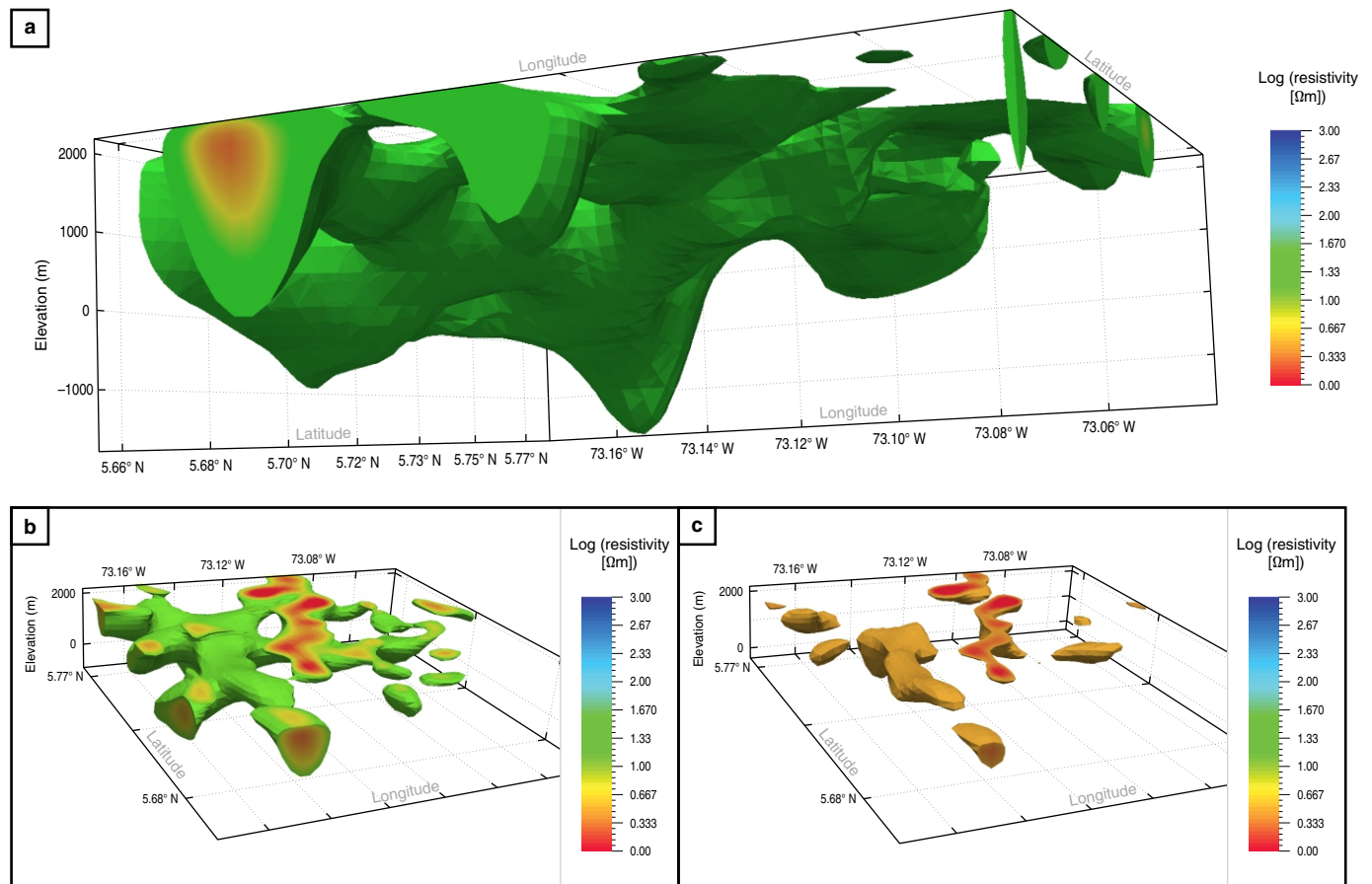
Figure 22. Volumetric view of the sedimentary cover with resistivity values that range between 0 and 80 Ω·m, **(a)** is the depth view and **(b)** the top view. This layer is thicker in the west and northwest. **(c)** is the top view of a layer in the sedimentary rocks that has high conductivity. This low resistivity (0–3 Ω·m) is probably due to the saline fluid circulation.

basosa–Toledo Anticline. The Une Formation provides permeability that influences fluid flow through the hydrothermal system.

Deep high angle faults (Paipa–Iza, Las Peñas, Agua Tibia, and Cerro Plateado Faults) and their intersections plus the contact zones between igneous intrusions and surrounding rocks represent controls that influence deep fluid circulation.

Clay layers from the Churuvita or Une Formations and from weathered pyroclastic deposits have low permeability and confine fluid flow within the sedimentary reservoir.

The magmatic heat source is located beneath the volcanic dome complexes and is associated with cooling and/or radiogenic heat production. In El Durazno Intrusive, the heat production is estimated from boreholes to be 12 μW/m^3, which could heat the water circulating through the northwest area, where a groundwater well discharges low salinity water at 34.8 °C. Although the dimensions of this intrusion have not been determined, the resistivity model shows that it is large at depth.

The chemical and isotopic composition of the hot springs is not representative of the geothermal fluid due to mixing with saline low temperature water. The existence of coal deposits and hydrocarbon seeps as well as the $\delta^{13}C_{CH4}$ values indicate

Figure 23. Volumetric view of the basement based on resistivity. **(a)** Metamorphic rocks and magmatic intrusions confined from 80 to 1000 Ω·m. **(b)** Intrusive rocks range from 500 to 1000 Ω·m.

contribution of organic components to the geothermal fluids. The input of magmatic/mantle gases is confirmed by the $\delta^{13}C_{CO2}$ and $^3He/^4He$ ratios.

The origin of the sodium sulfate saline water is the dissolution of a deep evaporite in the sedimentary sequence from the west and northwest sectors.

Secondary minerals, including epidote, adularia, albite, and biotite plus local occurrences of dickite reflect water–rock interaction between 200 °C and ca. 320 °C. Although aqueous and gas geothermometers are highly affected by mixing with fluids of different origins, a simple enthalpy–silica model suggests a current resource temperature of ca. 230 °C.

The gravity and magnetotelluric results show that igneous intrusions and metamorphic rocks in the basement are related to high density and high resistivity anomalies. The location of an igneous intrusion below the alto Los Volcanes appears to extend laterally northeast, giving rise to the alto Los Godos volcanic
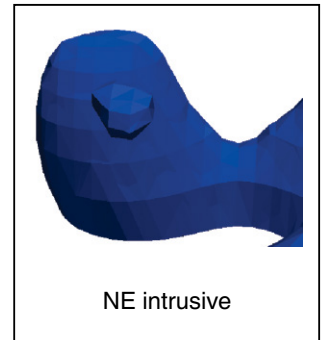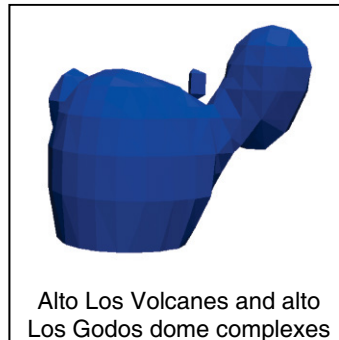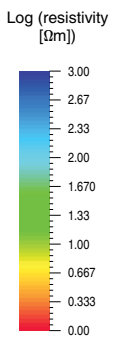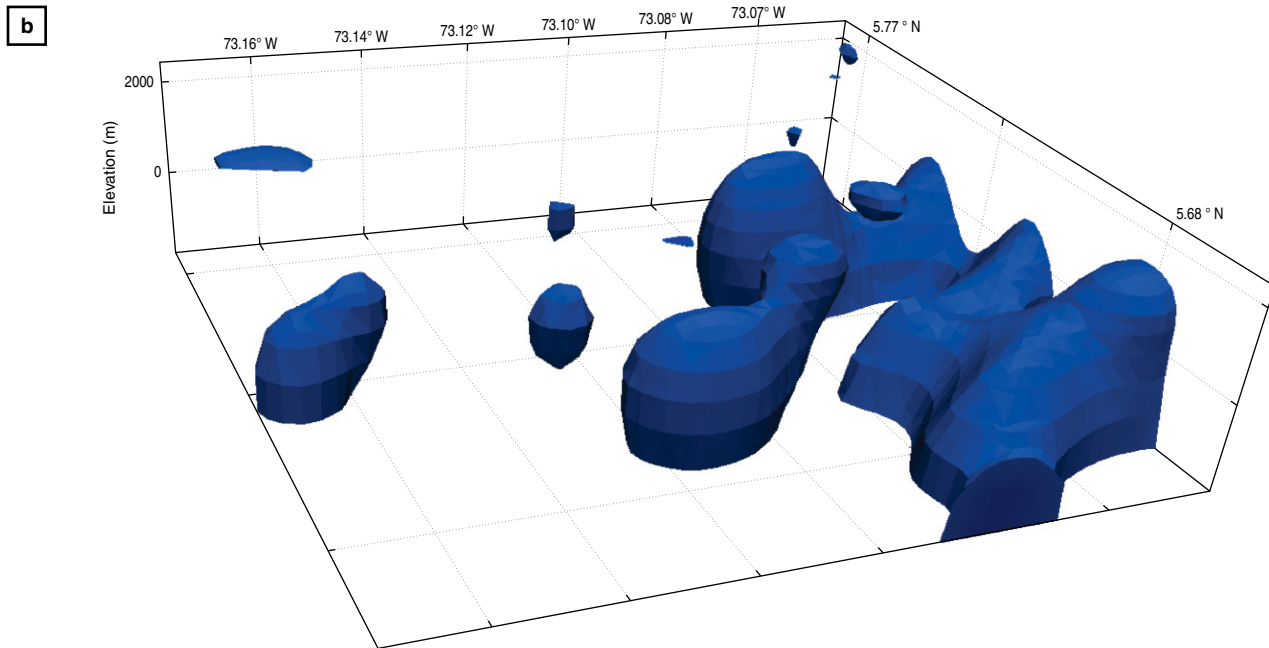
El Durazno Intrusive
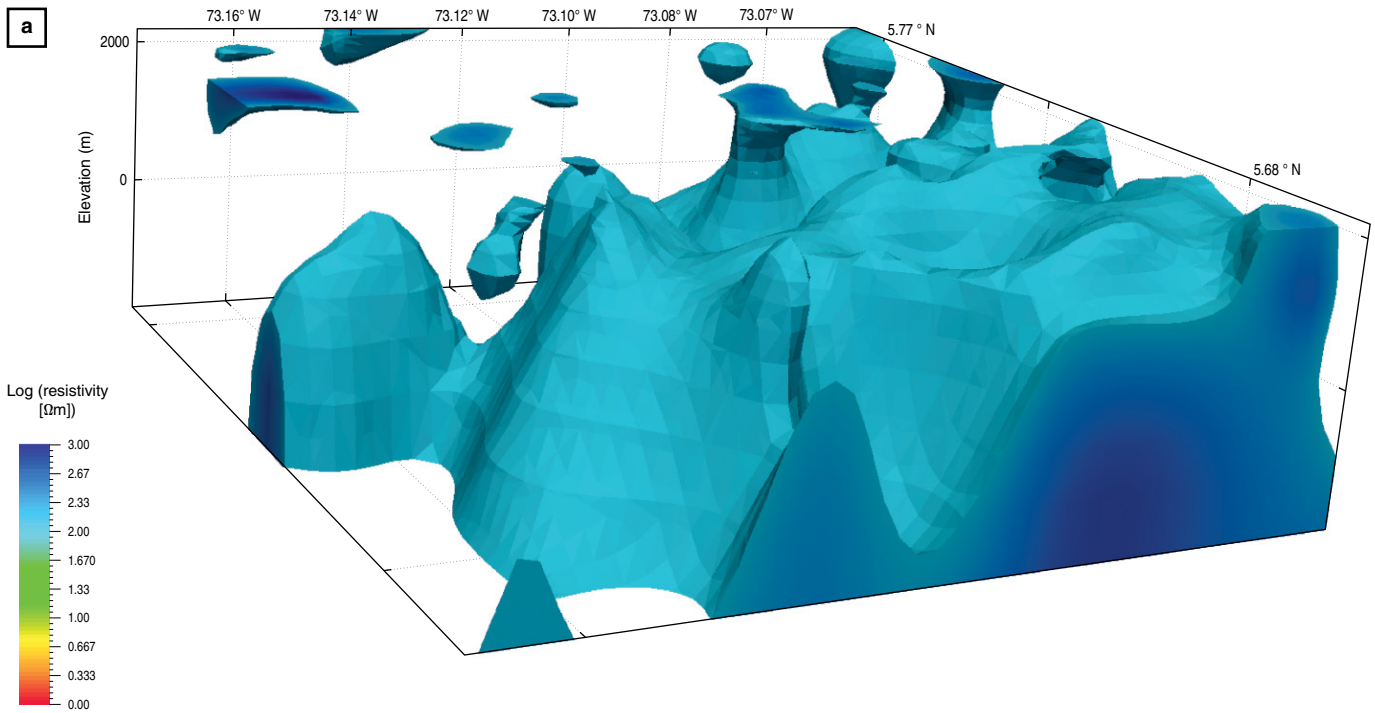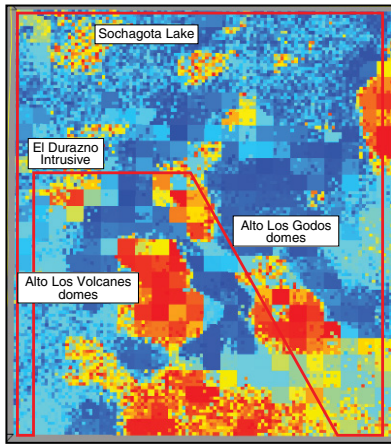
Alto Los Volcanes and alto
Los Godos dome complexes

NE intrusive

Table 4. Summary of evidence supporting the conceptual model.

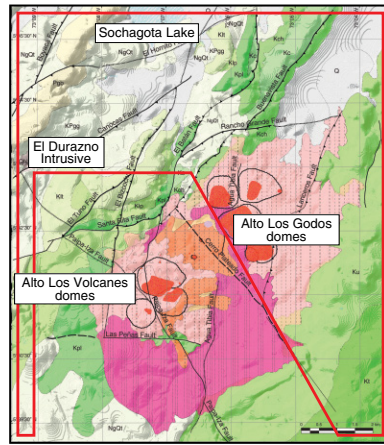| Geothermal system features	Evidences/signs	Source of information
Regional recharge zone	Terrain tilted from north to south	Topography–geology
	Hydraulic gradient between Tibasosa–Toledo Anticline and the valley	Topography–geology
	Sandstones outcrops from the Une Formation on the anticline	Geology
	Dipping strata from the Une Formation on the anticline	Structural geology
	Composition of the recharge water (ca. 2900 masl)	Isotope hydrology
Heat source	Hot magmatic intrusions from residual magmatic heat	Geology
	Radiogenic heat	Radioactive isotope geochemistry
	Possible recent intrusions without surface expression	Magnetic survey, magnetotellurics, geology, and isotopic helium geochemistry
Upflow zone	Contact between magmatic intrusions and surrounding rocks	Geology, magnetotellurics
	Vertical faults	Structural geology
Deep reservoir location	Basement xenoliths	Hydrothermal alteration
Reservoir temperature	Secondary minerals (up to 320 °C)	Hydrothermal alteration
	Enthalpy–silica model (up to 230 °C)	Fluid geochemistry
Sedimentary reservoir location	Availability of sandstones from the Une Formation between high density and high resistivity dome complexes	Geology, geological model, magnetotellurics
Deep infiltration conduits	Deep faults: Paipa–Iza, Las Peñas, and Aguatibia Faults; and intersection between them	Structural geology
	Contact between magmatic intrusions and surrounding rocks	Geology
Outflow (lateral circulation)	Lateral extension of the Une formation	Geology and geological model
	Occurrence of a discharge zone of limited permeability (very low flow rate)	Geology and geochemistry
Cap rock	Clayish levels within the sedimentary sequence (Churuvita and Une Formations)	Geology
	Weathered pyroclastic deposits	Geology
Discharge zone	Hot springs sites	Geology and geochemistry
	Steam vent	Geology and geochemistry
	Affected by mixing with a saline source (sodium sulfate)	Geochemistry
Geothermal fluid composition	Affected by mixing with organic carbon	Geochemistry, isotopic gas geochemistry, geology (coal mantles and seeps)
	Contribution of magmatic CO_2	Isotopic gas geochemistry
	Contribution of a high $^3He/^4He$ source	Isotopic gas geochemistry

dome complexes. In the middle of the geothermal area, a low density and intermediate resistivity volume surrounded by high density and high resistivity anomalies represents the sedimentary reservoir hosted by the Une Formation.

The characteristic resistivity of the intrusions suggests that they are mostly crystallized down to 4 km. However, the magmatic CO_2 source and $^3He/^4He$ ratio indicate a current magmatic/mantle contribution.
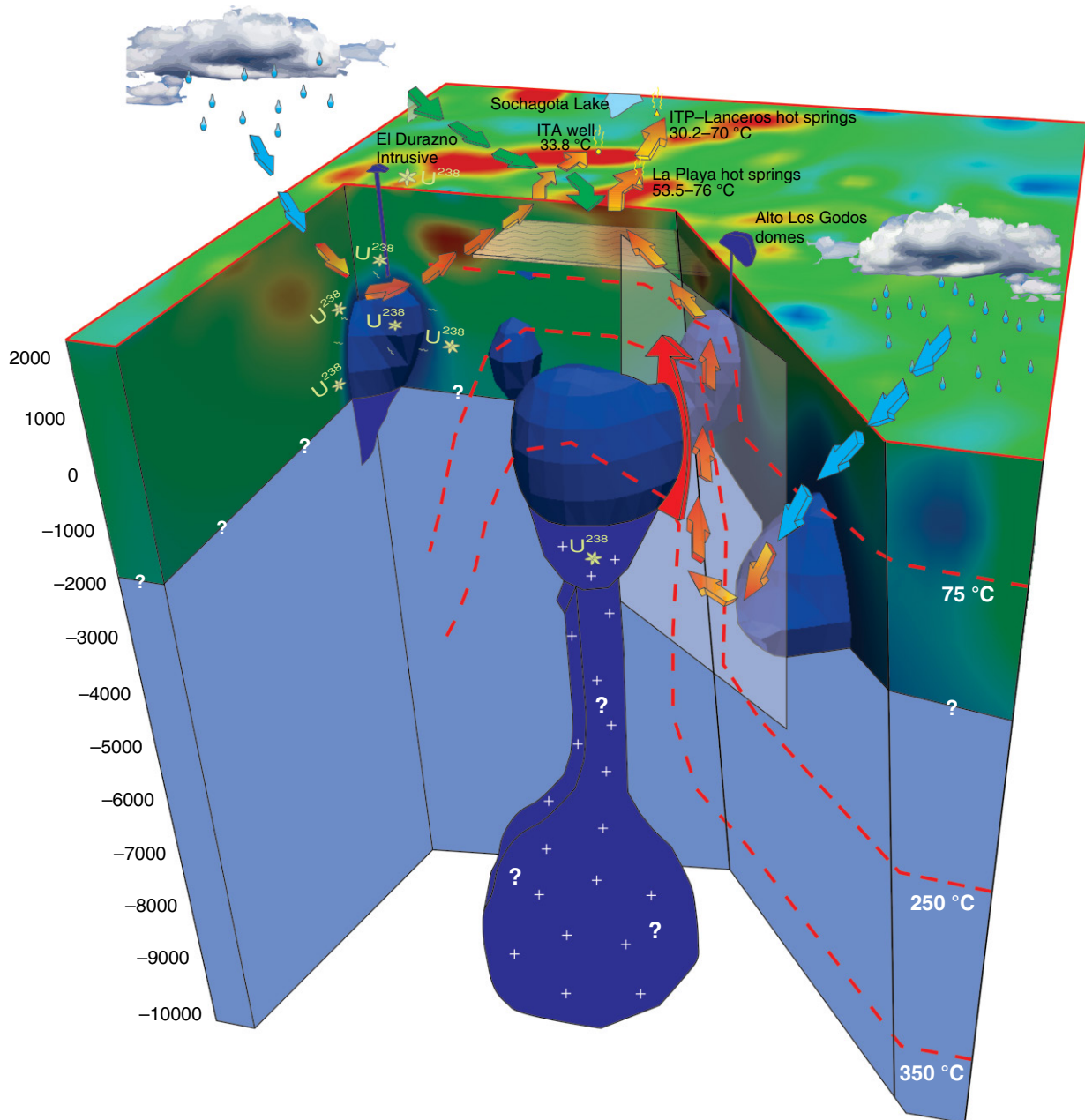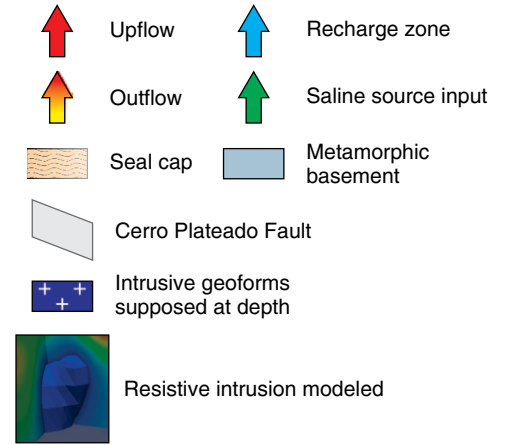
Figure 24. Conceptual model of the Paipa geothermal system. The main recharge zone is located in the western flank of the Tibasosa–Toledo Anticline, in the area where the Une Formation crops out. The deep circulation through high angle faults as well as the contacts of the magmatic intrusions, enriched in radioactive elements, causes the water temperature to increase. The upflow zone feeds the relatively shallow reservoir in the Une Formation. The outflow from this reservoir is favored by the Cerro Plateado Fault. The Une Formation provides permeability and fluid flow to the north until the main discharge zone (ITP–Lanceros sector) where the high vertical permeability conditions reach the surface. Saline water is mixed with the geothermal fluid along the outflow, masking its chemical and isotope composition.

Density map at a 2000 masl

Geological map

Upflow

Recharge zone

Outflow

Saline source input

Seal cap

Metamorphic basement

Cerro Plateado Fault

Intrusive geoforms supposed at depth

Resistive intrusion modeled

Sochagota Lake

El Durazno Intrusive

Alto Los Godos domes

Alto Los Volcanes domes

Sochagota Lake

El Durazno Intrusive

Alto Los Godos domes

Alto Los Volcanes domes

Sochagota Lake

ITA well
33.8 °C

ITP–Lanceros hot springs
30.2–70 °C

La Playa hot springs
53.5–76 °C

El Durazno
Intrusive

Alto Los Godos
domes

U^{238}

U^{238}

U^{238}

U^{238}

U^{238}

U^{238}

$+U^{238}$

2000

1000

0

−1000

−2000

−3000

−4000

−5000

−6000

−7000

−8000

−9000

−10000

75 °C

250 °C

350 °C

?

Acknowledgments

The authors express a very special thanks to the reviewers for the hard work undertaken in the careful revision of the manuscript of this chapter. Thanks to the professionals that during the development of this study took part of the Grupo de Exploración de Recursos Geotérmicos: Francisco, Wilson, Luis Eduardo, José Vicente, Natalia, Lina Fernanda, Héctor, María Teresa, Jaime, Edwin, Iván Darío, María Luisa, and Javier. Thanks to the chemists and geologists from the laboratories of the SGC, who participated in the analytical work. Additionally, thanks to the experts who along several years guided us and provided technical contributions to this study, particularly regarding geophysical methods and to the participants in an international panel for their comments, suggestions, and recommendations on the conceptual model. Finally, thanks to the local community for allowing us to learn about the fascinating Paipa geothermal system.

References

Alfaro, C. 2002a. Geoquímica del sistema geotérmico de Paipa. Ingeominas, 97 p. Bogotá.

Alfaro, C. 2002b. Estudio isotópico de aguas del área geotérmica de Paipa. Ingeominas, 15 p. Bogotá.

Alfaro, C. 2005a. Alteración hidrotermal en el sistema geotérmico de Paipa. Ingeominas, 53 p. Bogotá.

Alfaro, C. 2005b. Geoquímica preliminar de gases del sistema geotérmico de Paipa. Ingeominas, 40 p. Bogotá.

Alfaro, C. 2012. Evaluación de la composición isotópica del agua de precipitación en el área geotérmica Paipa–Iza. Ingeominas, 45 p. Bogotá.

Alfaro, C. 2015. Improvement of perception of the geothermal energy as a potential source of electrical energy in Colombia, country update. World Geothermal Congress 2015. Proceedings, 15 p. Melbourne, Australia.

Alfaro, C. & Espinosa, O. 2004. Sondeo preliminar de radón en el área geotérmica de Paipa. Ingeominas, 37 p. Bogotá.

Alfaro, C., Velandia, F., Cepeda, H., Pardo, N., Vásquez, L. & Espinosa, O. 2005. Modelo conceptual preliminar del sistema geotérmico de Paipa. Ingeominas, 42 p. Bogotá.

Alfaro, C., Ponce, P., Monsalve, M.L., Ortiz, I., Franco, J.V., Ortega, A., Torres, R. & Gómez, D. 2015. A preliminary conceptual model of Azufral geothermal system, Colombia. World Geothermal Congress 2015. Proceedings, 10 p. Melbourne.

Alfaro, C., Matiz–León, J.C., Rueda–Gutiérrez, J.B., Rodríguez–Rodríguez, G.F., González–Idárraga, C.E., Beltrán–Luque, M.A., Rodríguez–Ospina, G.Z. & Malo–Lázaro, J.E. 2017. Actualización del modelo conceptual del área geotérmica de Paipa. Servicio Geológico Colombiano, 111 p. Bogotá.

Alvarado, I., Alfaro, C. & Quintero, W. 2008. Mapa preliminar de gradientes geotérmicos (Método BHT). Scale 1:1 500 000. Ingeominas & Agencia Nacional de Hidrocarburos. Bogotá.

Beardsmore, G.R. & Cull, J.P. 2001. Crustal heat flow: A guide to measurement and modelling. Cambridge University Press, 324 p. Cambridge, USA. https://doi.org/10.1017/CBO9780511606021

Beltrán, M.A. 2015. Interpretación de anomalías magnetométricas y gravimétricas en el área geotérmica de Paipa–Iza. Servicio Geológico Colombiano, 123 p. Bogotá.

Bernet, M., Urueña, C., Amaya, S. & Peña, M.L. 2016. New thermo and geochronological constraints on the Pliocene – Pleistocene eruption history of the Paipa–Iza Volcanic Complex, Eastern Cordillera, Colombia. Journal of Volcanology and Geothermal Research, 327: 299–309. https://doi.org/10.1016/j.jvolgeores.2016.08.013

Bertrami, R., Camacho, A., De Stefanis, L., Medina, T. & Zuppi, G.M. 1992. Geochemical and isotopic exploration of the geothermal area of Paipa, cordillera Oriental, Colombia. Geothermal investigations with isotope and geochemical techniques in Latin America. Proceedings of a Final Research Coordination Meeting held in San José, Costa Rica. International Atomic Energy Agency, p. 169–199. Viena.

Boussingault, M. & Roulin. 1849. Viajes científicos a los Andes ecuatoriales ó colección de memorias sobre física, química e historia natural de la Nueva Granada, Ecuador y Venezuela. Lasserre Editorial, 322 p. Paris, France.

Cepeda, H. & Pardo, N. 2004. Vulcanismo de Paipa. Ingeominas, 103 p. Bogotá.

Colletta, B., Hebrard, F., Letouzey, J., Werner, P. & Rudkiewicz, J.L. 1990. Tectonic style and crustal structure of the Eastern Cordillera (Colombia) from a balanced cross–section. In: Letouzey, J. (editor), Petroleum and tectonics in mobile belts. Editions Technip, p. 81–100. Paris.

Cooper, M.A., Addison, F.T., Álvarez, R., Coral, M., Graham, R.H., Hayward, A.B., Howe, S., Martínez, J., Naar, J., Penas, R., Pulham, A.J. & Taborda, A. 1995. Basin development and tectonic history of the Llanos Basin, Eastern Cordillera, and Middle Magdalena Valley, Colombia. American Association of Petroleum Geologists Bulletin, 79(10): 1421–1443.

D'Amore, F. & Panichi, C. 1980. Evaluation of deep temperatures of hydrothermal systems by a new gas geothermometer. Geochimica et Cosmochimica Acta, 44(3): 549–556. https://doi.org/10.1016/0016-7037(80)90051-4

D'Amore, F. & Panichi, C. 1987. Geochemistry in geothermal exploration. In: Economides, M.J. & Ungemach, P.O. (editors), Applied Geothermics. John Wiley & Sons Ltd., 68–89. New York.

Dengo, C. & Covey, M.C. 1993. Structure of the Eastern Cordillera of Colombia: Implications for trap styles and regional tectonics. American Association of Petroleum Geologists Bulletin, 77(8): 1315–1337.

Empresa Nacional de Uranio S.A. & Instituto de Asuntos Nucleares. 1979. Reporte Contrato I. 51 p. Bogotá.

Empresa Nacional de Uranio S.A. & Instituto de Asuntos Nucleares. 1980. Reporte Contrato I. 51 p. Bogotá.

Fabre, A. 1983. La subsidencia de la cuenca del Cocuy (cordillera Oriental de Colombia) durante el Cretáceo y el terciario. Segunda Parte: Esquema de evolución tectónica. Geología Norandina, (8): 21–27.

Ferreira, P. & Hernández, G. 1988. Evaluación geotérmica en el área de Paipa basada en técnicas isotópicas, geoquímica y aspectos estructurales. Bachelor thesis, Universidad Nacional de Colombia, 125 p. Bogotá.

Fonseca, J.M. 2018. Monitoreo de caudales. Fuentes termominerales sector ITP, municipio de Paipa. Corpoboyacá, 47 p. Tunja.

Fournier, R.O. 1977. Chemical geothermometers and mixing models for geothermal systems. Geothermics, 5(1–4): 41–50. https://doi.org/10.1016/0375-6505(77)90007-4

Franco, J.V. 2012. Prospección geoeléctrica en los alrededores del volcán de Paipa, Boyacá. Servicio Geológico Colombiano, 54 p. Bogotá.

Franco, J.V. 2016. Actualización geoeléctrica en el área geotérmica de Paipa, Boyacá. Servicio Geológico Colombiano, 86 p. Medellín.

Garzón, T. 2003. Geoquímica y potencial minero asociado a cuerpos volcánicos en la región de Paipa, departamento de Boyacá, Colombia. Master thesis, Universidad Nacional de Colombia, 159 p. Bogotá.

Geocónsul. 1992. Evaluación geotérmica del Macizo Volcánico del Ruiz, Colombia. Final report, 57 p. Morelia, México.

Giggenbach, W.F. 1987. Redox processes governing the chemistry of fumarolic gas discharges from White Island, New Zealand. Applied Geochemistry, 2(2): 143–161. https://doi.org/10.1016/0883-2927(87)90030-8

Giggenbach, W.F. 1988. Geothermal solute equilibria. Derivation of Na–K–Mg–Ca geoindicators. Geochimica et Cosmochimica Acta, 52(12): 2749–2765. https://doi.org/10.1016/0016-7037(88)90143-3

Giggenbach, W.F. 1991. Chemical techniques in geothermal exploration. In: D'Amore, F. (editor), Application of geochemistry in geothermal reservoir development. UNITAR/UNDP Center on Small Energy Resources, p. 119–144. Rome.

Giggenbach, W.F. 1997. Relative importance of thermodynamic and kinetic processes in governing the chemical and isotopic composition of carbon gases in high–heatflow sedimentary basins. Geochimica et Cosmochimica Acta, 61(17): 3763–3785. https://doi.org/10.1016/S0016-7037(97)00171-3

Giggenbach, W.F. & Goguel, R.L. 1989. Collection and analysis of geothermal and volcanic water and gas discharges. 4th Edition. Department of Scientific and Industrial Research, Chemistry Division. Report CD 2401, 81 p. Petone, New Zealand.

Giggenbach, W.F., García, N., Londoño, A., Rodríguez, L., Rojas, N. & Calvache, M.L. 1990. The chemistry of fumarolic vapor and thermal–spring discharges from the Nevado del Ruiz volcanic–magmatic–hydrothermal system, Colombia. Journal of Volcanology and Geothermal Research, 42(1–2): 13–39. https://doi.org/10.1016/0377-0273(90)90067-P

González, L., Vásquez, L., Muñoz, R., Gómez, H., Parrado, G. & Vargas, S. 2008. Exploración de uranio en Paipa, Iza, Pesca, Chivatá (Boyacá). Ingeominas, 190 p. Bogotá.

González–Idárraga, C.E. & Rodríguez–Rodríguez, G.F. 2017. Modelo resistivo del área geotérmica de Paipa a partir de datos magnetotelúricos. Servicio Geológico Colombiano, 96 p. Bogotá.

Hernández, G. & Osorio, O. 1990. Geología, análisis petrográfico y químico de las rocas volcánicas del suroriente de Paipa, Boyacá, Colombia. Bachelor thesis, Universidad Nacional de Colombia, 100 p. Bogotá.

Hoefs, J. 1978. Some peculiarities in the carbon isotope composition of 'juvenile' carbon. In: Robinson, B.W. (editor), Stable isotope in the earth Sciences. Bulletin of the New Zealand Department of Industrial Research, 220, p. 181–184. Wellington, New Zealand.

Koga, A. 2000. Hydrothermal geochemistry: The first group training course on geothermal energy and environmental sciences. Kyushu University, class notes, 81 p. Fukuoka, Japan.

Ledo, J. 2005. 2–D versus 3–D magnetotelluric data interpretation. Surveys in Geophysics, 26(5): 511–543. https://doi.org/10.1007/s10712-005-1757-8

Llanos, E.M., Bonet, C. & Zengerer, M. 2015. 3D geological–geophysical model building and forward and inverse modeling of magnetism and gravimetry data from Paipa geothermal area, Colombia–Final report. Contract No 363 of 2015. Servicio Geológico Colombiano, 106 p. Melbourne.

Lozano, E. 1990. Avances en el conocimiento geotérmico del área de Paipa. Instituto Colombiano de Energía Eléctrica, reporte técnico, 9 p. Bogotá.

Lyon, G.L. & Hulston, J.R. 1984. Carbon and hydrogen isotopic compositions of New Zealand geothermal gases. Geochimica et Cosmochimica Acta, 48(6): 1161–1171. https://doi.org/10.1016/0016-7037(84)90052-8

Malo, J. & Alfaro, C. 2017. Línea meteórica local, Boyacá Centro Norte. Servicio Geológico Colombiano, 103 p. Bogotá.

Middleton, M.F. 1979. Heat flow in the Moomba, Big Lake and Toolachee gas fields of the Cooper Basin and implications for hydrocarbon maturation. Exploration Geophysics, 10(2): 149–155. https://doi.org/10.1071/EG979149

Mojica, J. & Villarroel, C. 1984. Contribución al conocimiento de las unidades paleozoicas del área de Floresta (cordillera Oriental colombiana; departamento de Boyacá) y en especial al de la Formación Cuche. Geología Colombiana, (13): 55–79.

Navia, A. & Barriga, A. 1929. Informe sobre las aguas termomedicinales de Paipa, Colombia. Gobernación de Boyacá, 76 p. Bogotá.

Ono, A., Sano, Y., Wakita, H. & Giggenbach, W. 1993. Carbon isotopes of methane and carbón dioxide in hydrothermal gases of Japan. Geochemical Journal, 27(4–5): 287–295. https://doi.org/10.2343/geochemj.27.287

Organización Latinoamericana de Energía, Instituto Colombiano de Energía Eléctrica, Consultoría Tecnológica Colombiana & Geotérmica Italiana. 1982. Estudio de reconocimiento de los recursos geotérmicos de la República de Colombia. Informe final, 46 p. Pisa, Italy.

Ortiz, I.D. & Alfaro, C. 2010. Inventario de puntos de agua y geoquímica de las áreas geotérmicas de Paipa e Iza: Aguas, suelos y peloides. Ingeominas, 118 p. Bogotá.

Panichi, C. & Gonfiantini, R. 1978. Environmental isotopes in geothermal studies. Geothermics, 6(3–4): 143–161. https://doi.org/10.1016/0375-6505(77)90024-4

Pearce, J.A., Harris, N.B.W. & Tindle, A.G. 1984. Trace element discrimination diagrams for the tectonic interpretation of granitic rocks. Journal of Petrology, 25(4): 956–983. https://doi.org/10.1093/petrology/25.4.956

Peccerillo, A. & Taylor, S.R. 1976. Geochemistry of Eocene calc–alkaline volcanic rocks from the Kastamonu area, Northern Turkey. Contributions to Mineralogy and Petrology, 58(1): 63–81. https://doi.org/10.1007/BF00384745

Renzoni, G. & Rosas, H. 1967. Geología de la plancha 171 Duitama. Scale 1:100 000. Ingeominas. Bogotá.

Renzoni, G., Rosas, H. & Etayo, F. 1998. Geología de la plancha 191 Tunja. Scale 1:100 000. Ingeominas. Bogotá.

Rodríguez, G. & Alfaro, C. 2015. Caracterización de núcleos de perforación en las zonas de El Durazno, Paipa y criptodomo de Iza. Servicio Geológico Colombiano, 84 p. Bogotá.

Rodríguez, G.F. & Vallejo, E.F. 2013. Informe final sondeos superficiales de temperatura en el área geotérmica de Paipa, Boyacá. Servicio Geológico Colombiano, 57 p. Bogotá.

Rueda, J. 2017. Cartografía de los cuerpos dómicos del área geotérmica de Paipa. Servicio Geológico Colombiano, 121 p. Bogotá.

Rueda, J. & Rodríguez, G. 2016. Geología del área geotérmica de San Diego, Caldas. Servicio Geológico Colombiano, 284 p. Bogotá.

Schoell, M. 1980. The hydrogen and carbon isotopic composition of methane from natural gases of various origins. Geochimica et Cosmochimica Acta, 44(5): 649–661. https://doi.org/10.1016/0016-7037(80)90155-6

Servicio Geológico Colombiano. 2015. Inventario nacional de manifestaciones hidrotermales. Aplicativo web: http://hidrotermales.sgc.gov.co/invtermales/ (consulted in November 2019).

Truesdell, A.H. & Fournier, R.O. 1977. Procedure for estimating the temperature of a hot water component in a mixed water by using a plot of dissolved silica versus enthalpy. Journal of Research of the U. S. Geological Survey, 5(1): 49–52.

van Leeuwen, W.A. 2016. Geothermal exploration using the magnetotelluric method. Utrecht University, Utrecht Studies in Earth Sciences 115, 277 p. Utrecht, the Netherlands.

Vásquez, L.E. 2002. Exploración geofísica con el método electromagnético en el municipio de Paipa. Ingeominas, 134 p. Bogotá.

Vásquez, L.E. 2012. Aplicación geofísica de métodos potenciales en el área geotérmica de Paipa–Iza. Servicio Geológico Colombiano, 93 p. Bogotá.

Velandia, F. 2003. Cartografía geológica y estructural sector sur del municipio de Paipa. Ingeominas, 31 p. Bogotá.

Wannamaker, P.E. 1999. Affordable magnetotellurics: Interpretation in natural environments. In: Oristaglio, M. & Spies, B. (editors), Three–dimensional electromagnetics. Society of Exploration Geophysicists, Geophysical Development, Series 7, p. 349–374. Tulsa, Oklahoma. https://doi.org/10.1190/1.9781560802154.ch22

Explanation of Acronyms, Abbreviations, and Symbols:

AMT	Audio–magnetotellurics		TDS	Total dissolved solids
ITP	Instituto de Turismo de Paipa		VAG	Volcanic arc granites
MT	Magnetotellurics		VES	Vertical electrical soundings
SGC	Servicio Geológico Colombiano		XRD	X–ray diffraction

Authors' Biographical Notes

Claudia María ALFARO–VALERO[1] has a BS in chemistry, Universidad Nacional de Colombia, and a postgraduate in geothermal technology, from the University of Auckland, New Zealand. Her research focuses on the geochemistry of hydrothermal and volcanic fluids and on geothermal exploration. She currently works as chief of the Grupo de Exploración de Recursos Geotérmicos.

Jesús Bernardo RUEDA–GUTIÉRREZ[2] has a BS geologist, Universidad Industrial de Santander, with experience in geological mapping, research on mineral exploration, volcanology, structural geology, and lithogeochemistry. He currently works as a geologist in the Grupo de Exploración de Recursos Geotérmicos of the Servicio Geológico Colombiano.

Jhon Camilo MATIZ–LEÓN[3] has a BS in cadastral and geodetic engineer, and a MS in information sciences and geomatics from Universidad Distrital Francisco José de Caldas. He previously worked as a remote sensing researcher for the executive secretary of the Comisión Colombiana del Espacio (CCE), under the responsibility of Instituto Geográfico Agustín Codazzi (IGAC), and has served as technical coordinator and zone leader for private companies in projects of digital mapping, geographic information systems (GIS), and satellite image processing for earth observation. He is currently working as a researcher in 3D modeling, in litho–constrained geophysical inversion and geomatics for the Grupo de Exploración de Recursos Geotérmicos of the Servicio Geológico Colombiano.

Miguel Angel BELTRÁN–LUQUE[4] has BS in geologist and a MS in geophysics from Universidad Nacional de Colombia with experience in the mining industry and in geologic exploration in areas such as the northern Cauca valley, northern Colombia ultramafic bodies (part of the Western Cordillera), the Middle Magdalena Valley, and the Central and Eastern Cordilleras. He currently works at the Servicio Geológico Colombiano in the Grupo de Exploración de Recursos Geotérmicos processing magnetic/gravimetric data from geothermal areas and undertaking active gravity and magnetic acquisitions in the San Diego geothermal area.

Gilbert Fabián RODRÍGUEZ–RODRÍGUEZ[5] has BS in cadastral and geodetic engineer from Universidad Distrital Francisco José de Caldas of Bogotá. He currently works in the Grupo de Exploración de Recursos Geotérmicos of the Servicio Geológico Colombiano as a researcher in geophysical sciences, with emphasis in shallow temperature surveys, magnetotelluric and TDEM surveys, and vertical electrical soundings.

Gina Z. RODRÍGUEZ–OSPINA[6] has a BS in geologist from Universidad Industrial de Santander, with experience in well logging, inventories of thermal springs, and cartography. She currently works in the Grupo de Exploración de Recursos Geotérmicos of the Servicio Geológico Colombiano in the acquisition, processing, and interpretation of structural data integrated into the geological mapping of geothermal areas.

Carlos Eduardo GONZÁLEZ–IDÁRRAGA[7] has a BS in physical engineer from Universidad Nacional de Colombia and a MS in Earth sciences from Institute of Geophysics of the Universidad Nacional Autónoma de México (UNAM), emphasizing the exploration of natural resources employing electromagnetic methods. He currently works as a geophysicist in the Grupo de Exploración de Recursos Geotérmicos of the Servicio Geológico Colombiano in the acquisition, processing, and interpretation of resistive models from magnetotelluric and TEM data.

Jaison Elías MALO–LÁZARO[8] has a BS in chemistry from Universidad de Córdoba and a specialization degree in instrumental chemical analysis at the Pontificia Universidad Javeriana. He currently works in the Grupo de Exploración de Recursos Geotérmicos of the Servicio Geológico Colombiano, supporting studies of fluid geochemistry, measurements of radon gas, and isotopy.